APRIL 2025
No 344

Authors
Thanh Nguyen-Xuan
Dzung Nguyen-Le
Quan Tran-Anh
Tung Nguyen-Duy
Thanh Ngo-Duc

Coordination
Marie-Noëlle Woillez

Research papers

Assessment of Future Droughts in Vietnam Using High-Resolution Downscaled CMIP6 Projections

ÉDITIONS AFD
AGENCE FRANÇAISE DE DÉVELOPPEMENT

Agence française de développement

Papiers de recherche

Les *Papiers de Recherche de l'AFD* ont pour but de diffuser rapidement les résultats de travaux en cours. Ils s'adressent principalement aux chercheurs, aux étudiants et au monde académique. Ils couvrent l'ensemble des sujets de travail de l'AFD : analyse économique, théorie économique, analyse des politiques publiques, sciences de l'ingénieur, sociologie, géographie et anthropologie. Une publication dans les *Papiers de Recherche de l'AFD* n'en exclut aucune autre.

Les opinions exprimées dans ce papier sont celles de son (ses) auteur(s) et ne reflètent pas nécessairement celles de l'AFD. Ce document est publié sous l'entière responsabilité de son (ses) auteur(s) ou des institutions partenaires.

Research Papers

AFD Research Papers are intended to rapidly disseminate findings of ongoing work and mainly target researchers, students and the wider academic community. They cover the full range of AFD work, including: economic analysis, economic theory, policy analysis, engineering sciences, sociology, geography and anthropology. *AFD Research Papers* and other publications are not mutually exclusive.

The opinions expressed in this paper are those of the author(s) and do not necessarily reflect the position of AFD. It is therefore published under the sole responsibility of its author(s) or its partner institutions.

Assessment of Future Droughts in Vietnam Using High-Resolution Downscaled CMIP6 Projections

Authors

Thanh Nguyen-Xuan
Department of Space and Applications, University of Science and Technology of Hanoi (USTH), Vietnam Academy of Science and Technology (VAST), Hanoi, Vietnam

Dzung Nguyen-Le
Department of Space and Applications, University of Science and Technology of Hanoi (USTH), Vietnam Academy of Science and Technology (VAST), Hanoi, Vietnam

Quan Tran-Anh
Hanoi University of Mining and Geology (HUMG), Hanoi, Vietnam

Tung Nguyen-Duy
Oxford University Clinical Research Unit, Ho Chi Minh city, Vietnam

Thanh Ngo-Duc*
Department of Space and Applications, University of Science and Technology of Hanoi (USTH), Vietnam Academy of Science and Technology (VAST), Hanoi, Vietnam.
ngo-duc.thanh@usth.edu.vn

*Corresponding author

Coordination

Marie-Noëlle Woillez (Agence française de développement)

Abstract
This study investigates drought conditions in Vietnam and its seven sub-climatic regions using the Standardized Precipitation-Evapotranspiration Index (SPEI). SPEI was derived from daily, high-resolution (10-km) precipitation and temperature products from the CMIP6-VN dataset, which statistically downscaled CMIP6 global models. Performance evaluation of 22 CMIP6-VN models confirmed their accuracy in representing precipitation and temperature characteristics for the reference period (1985–2014). Regarding the future period (2015–2099) under three Shared Socioeconomic Pathways (SSPs) (SSP1-2.6, SSP2-4.5, and SSP5-8.5), significant warming is projected across Vietnam, while precipitation projections remain uncertain, with most areas anticipated to experience slightly increased rainfall. SPEI results indicate that precipitation significantly influences drought conditions more than temperature, accounting for approximately 70% of the SPEI trend under SSP5-8.5, which consequently introduces substantial uncertainty in drought projections. Drought conditions under different global warming levels (GWLs) were investigated, showing that while drought may not occur more frequently at high GWLs, more extreme drought events are projected. Five models exhibiting the most pronounced increasing drought trends were further analyzed, revealing a deterioration of all drought characteristics, particularly in the Northwest, Northeast, and Central Highlands. Copula statistical analysis reveals that drought events with higher return periods tend to be more prolonged and severe in the future.

Keywords
Drought; Statistical Downscaling; CMIP6; SSP scenarios; Vietnam; Climate Change

Acknowledgements
This study is supported by the 2nd phase of the GEMMES Vietnam project, funded by the French Development Agency (AFD) through Facility 2050, and the Vietnam National Foundation for Science and Technology Development (NAFOSTED) under Grant 105.06-2021.14. We would like to express our special thanks to Dr. Marie-Noëlle Woillez from AFD for her careful review and valuable suggestions to improve this manuscript.

Original version
English

Accepted
March 2025

Résumé
Cette étude examine les conditions de sécheresse au Vietnam et dans ses sept sous-régions climatiques à l'aide de l'Indice Standardisé de Précipitations et d'Évapotranspiration (SPEI). Le SPEI est dérivé de données quotidiennes de précipitations et de températures à haute résolution (10 km) issues du jeu de données CMIP6-VN, lequel est obtenu par descente d'échelle statistique des modèles globaux CMIP6. L'évaluation des performances de 22 modèles CMIP6-VN a confirmé leurs bonnes capacités dans la représentation des caractéristiques des précipitations et des températures pour la période de référence (1985–2014). Concernant la période future (2015–2099) selon trois Scénarios Socioéconomiques Partagés (SSP) (SSP1-2.6, SSP2-4.5 et SSP5-

8.5), un réchauffement significatif est projeté sur l'ensemble du Vietnam, tandis que les projections des précipitations restent incertaines, bien que la plupart des régions anticipent une légère augmentation des précipitations. Les résultats du SPEI indiquent que les précipitations influencent les conditions de sécheresse de manière plus significative que la température, représentant environ 70 % de la tendance du SPEI sous le scénario SSP5-8.5, ce qui introduit ainsi une incertitude substantielle dans les projections de sécheresse. Les conditions de sécheresse sous différents niveaux de réchauffement global (GWL) ont été examinées, révélant que, bien que la fréquence des sécheresses ne soit pas nécessairement plus élevée aux niveaux de réchauffement élevés, davantage d'épisodes extrêmes sont projetés. Cinq modèles présentant les tendances de sécheresse les plus marquées ont été analysés plus en détail, mettant en évidence une détérioration de toutes les caractéristiques des sécheresses, en particulier dans le Nord-Ouest, le Nord-Est et les Hauts Plateaux du Vietnam. L'analyse statistique par copules révèle que les événements de sécheresse avec des périodes de retour plus élevées tendent à être plus prolongés et plus sévères dans le futur.

Mots-clés
Sécheresse; Descente d'échelle statistique; CMIP6; Scénarios SSP; Vietnam; Changement Climatique

Remerciements
Cette étude est soutenue par la deuxième phase du projet GEMMES Vietnam, financé par l'Agence Française de Développement (AFD) via le Facilité 2050, ainsi que par la Fondation nationale vietnamienne pour le développement de la science et de la technologie (NAFOSTED) dans le cadre de la subvention 105.06-2021.14. Nous souhaitons exprimer nos remerciements spéciaux au Dr. Marie-Noëlle Woillez de l'AFD pour sa relecture attentive et ses précieuses suggestions visant à améliorer ce manuscrit.

Version originale
Anglais

Acceptée
Mars 2025

1. Introduction

Vietnam, a Southeast Asian developing country with a dense population of approximately 100 million, has come to play an important role in global food production (WTO, 2023). According to the Food and Agriculture Organization of the United Nations (FAO) Statistics (FAO, 2022), Vietnam is the world's fifth-largest producer of rice, the fourth-largest producer of cashew nuts, and the sixth-largest producer of tea. Notably, the country is the largest producer of black pepper, accounting for one-third of the global market, the second-largest producer of cinnamon and coffee, and the third-largest producer of rubber and spices in the world (MARD, 2024). Furthermore, Vietnam is a major exporter of other agricultural products, including cotton, peanuts, sugarcane, and walnuts. As highlighted in the 2021 United Nations Food System Summit (UNFSS) dialogue, Vietnam's agricultural sector not only meets domestic food demands but also significantly contributes to global food security (UNFSS, 2021). Leveraging these strengths, the country aims to rank among the world's top ten in agricultural production by 2050, with a focus on a modern, efficient, and environmentally friendly agricultural processing industry (MPI, 2021).

However, anthropogenic global climate change poses a serious threat to Vietnam's agricultural sector (World Bank Group, 2022). Similar to other Southeast Asian countries, Vietnam has experienced volatility in food supply due to climate change (Dao and Nguyen, 2022). For a country whose economy heavily depends on agricultural production, like Vietnam, the increasing frequency and intensity of water-related extreme climate events, such as droughts, exacerbate the risk of severe agricultural damage.

Drought is a natural hazard caused by a prolonged deficiency in precipitation relative to normal expectations. As this shortage persists, it fails to meet the water demands of both human activities and the environment. There are various ways to classify droughts, but they are primarily categorized based on two approaches: considering drought as a physical phenomenon or via its impacts on socio-economic systems. Despite the difficulty of defining drought objectively, which has led to the development of a large number (>100) of different drought indices (Lloyd-Hughes, 2014), droughts are commonly classified into meteorological, hydrological, agricultural, and socio-economic droughts (Wilhite and Glantz, 1985). Unlike rapid-onset natural hazards such as earthquakes, droughts develop gradually and can often be monitored and forecasted based on their strong connections to rainfall, temperature, and other meteorological variables (Wilhite, 2000; Fahim et al., 2016). While meteorological droughts are primarily caused by precipitation deficits, growing evidence indicates that increased temperature can significantly intensify their severity, duration, and spatial extent (Vicente-Serrano et al., 2010; Dai, 2011; Cook et al., 2014; Trenberth et al., 2014; Diffenbaugh et al., 2015). Thus, studies that employ solely precipitation-based indices, such as the Standardized Precipitation Index (SPI) (McKee et al., 1993) and the Effective Drought Index (EDI) (Byun and Wilhite, 1999), may underestimate future drought risks by not accounting for the crucial role of temperature (Dai, 2011; Trenberth et al., 2014). Moreover, there is evidence suggesting that precipitation projections still have substantially higher uncertainties compared to temperature projections, especially at the regional scale (Gao et al., 2016; Persad et al., 2020; Zappa et al., 2021; Kotz et al., 2024). To address the limitations of precipitation-only metrics, the comprehensive Standardized Precipitation Evapotranspiration Index (SPEI) was developed. The SPEI is highly effective since it integrates both precipitation and atmospheric evaporative demand, where the latter can be estimated using temperatures and extraterrestrial radiation, both of which influence drought persistence (Vicente-Serrano et al., 2010, 2014; Beguería et al., 2014). It represents a robust tool for retrospectively assessing historical droughts and prospectively projecting future changes, offering advantages over indices focused solely on precipitation.

Vietnam's susceptibility to drought has been well-documented, given its largely agricultural economy and the profound impact of water availability fluctuations on millions of

livelihoods. Droughts are ranked as the third most costly natural hazard in Vietnam, frequently causing substantial economic losses (Nguyen and Shaw, 2011). Over the past few decades, the country has faced several severe drought events. According to the National Action Programme (NAP) to Combat Desertification (MARD, 2002), from 1976 to 1998, droughts seriously affected 11 crop seasons in Vietnam, leading to extensive damage, including the destruction of hundreds of thousands of hectares of rice, coffee, tea, and fruits. Notably, the 1997–1998 drought event affected about 3.8 million people with freshwater shortages and resulted in total losses and damages exceeding $500 million in Vietnam (MARD, 2002). The 2015–2016 episode resulted in an estimated $670 million in damages and left nearly 2 million people grappling with water scarcity (Le et al., 2021; Ha et al., 2021; FAO, 2024). Both events were related to major El Niño events. More recently, an unprecedented drought occurred in 2019–2020, despite a weak El Niño event, and exacerbated water shortages across the country (OSNSC, 2021). Given that global and regional climate models consistently project rising temperatures, erratic precipitation patterns, and increased drought risks across the Southeast Asian mainland (Dai, 2011; Prudhomme et al., 2014; Arnell and Gosling, 2016; Naumann et al., 2018), there is an urgent imperative to comprehensively assess potential future drought emergencies in Vietnam.

The Paris Agreement of 2015 aims to limit global warming by the end of the 21st century to well below 2°C above pre-industrial levels while striving to restrict the increase to 1.5°C. Scientists have warned that if global temperatures rise beyond 2°C, humanity and ecosystems will face severe threats (IPCC, 2021). However, according to the last United Nations Emission Gap Report (2024) "*Countries are still off track to deliver on the globally insufficient mitigation pledges for 2023*" and current policies could lead to more than 3°C warming by the end of the century. Developing climate projections, including extreme events, is therefore essential. In Vietnam, while SPEI has been recently employed to examine historical drought occurrences (e.g., Le et al., 2019; Le et al., 2020; Phan-Van et al., 2022), there remains a crucial gap in knowledge regarding comprehensive multi-scenario projections that integrate SPEI with the latest high-resolution climate model outputs. This gap is especially significant considering Vietnam's diverse hydroclimatic gradients, which range from tropical monsoon regimes in the south to more temperate conditions in the northern uplands. Therefore, the objective of this study is to assess the future changes in drought occurrences in Vietnam based on the most up-to-date detailed climate projection data. In particular, we will focus on analyzing these changes under different global warming scenarios, ranging from 1.5°C to 4°C above the pre-industrial level. The rest of the paper is organized as follows: Section 2 presents the study area, data sources, and methods; Section 3 discusses the results, and the conclusions are presented in Section 4.

2. Materials and Methods

2.1. Studied regions

In this study, we focus on Vietnam and its seven sub-climatic regions (Figure 1). These sub-climatic regions — Northwest (R1), Northeast (R2), Red River Delta (R3), North Central (R4), Central South (R5), Central Highlands (R6), and Southern (R7) — are categorized based on variations in radiation and temperature, which differentiate the North domain (R1–R4) from the South domain (R5–R7), as well as differences in rainfall, which further distinguish sub-climatic regions (Nguyen and Nguyen, 2004).

Figure 1. Topography of Vietnam and location of the seven sub-climatic regions.

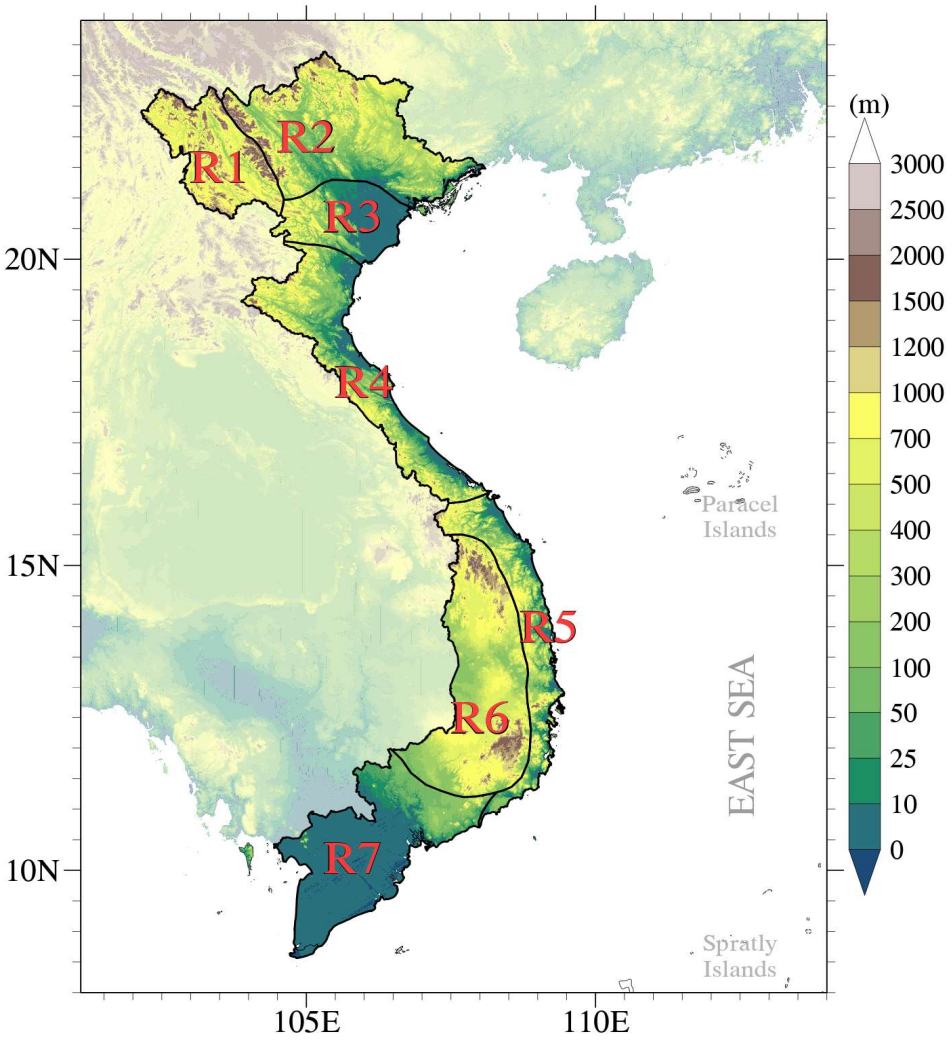

Source: Authors' own visualization. Original. The topography data is extracted from Hydroshed data (NASA SRTM, 2013).

2.2. CMIP6-VN: a downscaled dataset for Vietnam

To conduct an in-depth analysis of future droughts across the seven sub-climatic regions of Vietnam, a high-resolution dataset is indispensable. This is particularly crucial as certain regions, such as parts of Region R4 and most of R5, span a relatively narrow longitudinal range, with some areas encompassing less than 0.5 degrees (corresponding to approximately 50 km) (Figure 1). It is noteworthy that while the widely used Coupled Model Intercomparison Project Phase 6 (CMIP6) global climate projections data (Eyring et al., 2016) have demonstrated their substantial role in various climate-related studies, their relatively coarse resolution restricts their applicability to local and regional scales, such as the area of interest in our study.

A recent study by Tran-Anh et al. (2023) introduced a new CMIP6-downscaled dataset for Vietnam using the Bias Correction and Spatial Disaggregation (BCSD) technique. The dataset, named CMIP6-VN, contains the downscaled outputs of 35 global climate models (GCMs) from both Tier-1 and Tier-2 CMIP6 experiments (Riahi et al. 2017) at a high spatial resolution of 0.1°×0.1° (~10 km), with a daily time step, covering the reference period 1980-2014 and the future period 2015-2099[1]. Note that the Tier 1 CMIP6 experiments consist of four 21st century Shared Socioeconomic Pathways (SSP) scenarios (SSP1-2.6, SSP2-4.5, SSP3-7.0, and SSP5-8.5), providing continuity with CMIP5 experiments by targeting a similar level of global radiative forcing. The Tier 2 experiments include more SSPs, such as SSP1-1.9 (to address the Paris Agreement target of 1.5°C), SSP4-3.4 (a gap-filling mitigation scenario), SSP4-6.0 (an update of RCP6.0), and SSP5-3.4OS (overshoot, testing the efficacy of certain mitigation measures) (Riahi et al., 2017). The performance of CMIP6-VN has been demonstrated for both precipitation and temperature. More importantly, the use of a large number of GCMs provides the ability to estimate the uncertainties of climate projections related to inter-model spread, including extreme climate events.

To identify drought conditions, a widely employed method is the utilization of rainfall-related indices, which are primarily constructed based on the deficiency of rainfall over a predetermined period (e.g. Vu-Thanh et al., 2014). However, several studies have highlighted the significance of considering temperatures, which drive evapotranspiration, in drought-estimation indices. Ignoring temperatures in these indices can result in a substantial underestimation of drought conditions (AghaKouchak et al., 2014; Diffenbaugh et al., 2015; Easterling et al., 2007; Griffin & Anchukaitis, 2014; Im et al., 2012; Kelley et al., 2015). Therefore, our study uses the SPEI index that incorporates both rainfall and temperature (including daily mean, daily maximum, and daily minimum temperatures, see section 2.3) obtained from CMIP6-VN. We conduct the analysis for three global greenhouse gas emission scenarios: 1) a sustainable development pathway (SSP1-2.6), with a focus on low-carbon policies; 2) a middle-of-the-road scenario (SSP2-4.5), where global development continues without significant changes to existing policies or economic growth patterns; and 3) a high-emissions pathway (SSP5-8.5). It is important to note that the best estimates of future global warming levels are 1.7°C, 2.0°C and 2.4°C above pre-industrial period for mid-term (2041-2060) and 1.8°C, 2.7°C and 4.4°C for long-term (2081-2100) under SSP1-2.6, SSP2-4.5, and SSP5-8.5 scenarios respectively (IPCC, 2021). Since CMIP6-VN does not provide full downscaling for all 35 GCMs across these three scenarios and for both rainfall and temperatures, we opted to use a subset of CMIP6-VN for this study, which includes downscaled products from only 22 GCMs (Table 1). For clarity, from henceforth, whenever we refer to the term "model" or the name of a specific GCM, we are referring to its corresponding downscaled product within the CMIP6-VN dataset.

[1] Although 2015 is now in the past, it was considered the future at the time the climate simulations were initiated, as they projected "future" conditions based on scenarios starting from 2015.

Table 1. List of the 22 downscaled CMIP6 GCMs from the CMIP6-VN dataset used in this study.

N°	GCM	Original Resolution (lat. × lon.)	Member Variant
1	ACCESS-CM2	1.88°×1.25°	r1i1p1f1
2	ACCESS-ESM1-5	1.88°×1.25°	r1i1p1f1
3	AWI-CM-1-1-MR	0.93°×0.94°	r1i1p1f1
4	BCC-CSM2-MR	1.13°×1.13°	r1i1p1f1
5	CMCC-ESM2	1.25°×1.25°	r1i1p1f1
6	CNRM-CM6-1-HR	1.25°×0.94°	r1i1p1f1
7	CNRM-ESM2-1	0.5°×0.5°	r1i1p1f2
8	CanESM5	1.41°×1.39°	r1i1p1f2
9	EC-Earth3	0.7°×0.7°	r1i1p1f1
10	EC-Earth3-Veg	0.7°×0.7°	r1i1p1f1
11	FGOALS-g3	2°×2.03°	r1i1p1f1
12	GFDL-ESM4	1°×1°	r1i1p1f1
13	GISS-E2-1-G	2.5°×2.5°	r1i1p1f2
14	HadGEM3-GC31-LL	1.88°×1.88°	r1i1p1f3
15	INM-CM5-0	2°×1.5°	r1i1p1f1
16	IPSL-CM6A-LR	2.5°×1.27°	r1i1p1f1
17	MIROC-ES2L	1.41°×1.41°	r1i1p1f1
18	MIROC6	2.81°×2.77°	r1i1p1f2
19	MPI-ESM1-2-HR	0.94°×0.94°	r1i1p1f1
20	MRI-ESM2-0	1.13°×1.13°	r1i1p1f1
21	NESM3	1.88°×1.88°	r1i1p1f1
22	UKESM1-0-LL	1.88°×1.25°	r1i1p1f2

2.3. Drought index: SPEI

Our study employs the Standardized Precipitation-Evapotranspiration Index (SPEI), which integrates the impacts of both precipitation and temperature (Vincente-Serrano et al., 2010; Beguería et al., 2014). The three main steps for calculating SPEI at scale of 12-month are outlined below.

- **Step 1:** Estimation of potential evapotranspiration (PET)

Potential evapotranspiration is the amount of water that would be evaporated given the meteorological conditions, assuming no water limitation. Various methods, including the Thornthwaite (Thornthwaite, 1948), the Hargreaves (Hargreaves, 1994), and the more intricate Penman-Monteith method (Allen et al., 1998), can be employed to estimate PET. However, the Thornthwaite method may overestimate PET and then overestimate drought events (Sheffield et al., 2012), while the Penman-Monteith method necessitates extensive data that is not included in CMIP6-VN (e.g., humidity, air pressure, wind speed, radiation, etc.). Consequently, this study employs a modified version of the Hargreaves method, incorporating adjustments that bring it closer to the Penman-Monteith method (Droogers and Allen, 2002; Beguería et al., 2014; Fu et al., 2023):

$$PET = 0.0013 \times 0.408 R_a \times (T_{avg} + 17.0) \times (TD - 0.0123P)^{0.76} \quad (1)$$

where PET is the potential evapotranspiration (mm/month), R_a is the extraterrestrial radiation (estimated from the latitude and the month of the year) ($MJm^{-2}day^{-1}$); T_{avg} is the monthly average temperature; TD is the temperature range (°C), calculated as the monthly average of the difference between daily maximum temperature and minimum temperature; P is precipitation (mm/month).

- **Step 2:** Determination of the climatic water balance (CWB) by subtracting PET from precipitation for each month.

$$CWB = P - PET \quad (2)$$

- **Step 3**: Estimation of SPEI-12

We then compute the 12-month accumulation of CWB by moving along the CWB series. A log-logistic probability distribution is subsequently fitted to the 12-month cumulative CWB values. Finally, the cumulative probability of the fitted distribution is transformed into standard normal values to derive the SPEI (referred to as SPEI-12), thereby standardizing the index for comparative analysis across various regions and timescales.

Drought events are identified when the SPEI-12 value falls below a threshold, typically set at -0.5, for a continuous period of at least two months, as established in previous studies (Wang et al., 2014; Sun et al., 2021; Yue et al., 2021). The five common drought characteristics (i.e., frequency, severity, duration, intensity, and inter-arrival time) are subsequently defined and illustrated in Figure 2. In essence, frequency refers to the number of drought events that occur during the study period. Severity is calculated as the sum of SPEI-12 absolute values below -0.5 for each drought event, and duration is the length of time (in months) that SPEI-12 remains below this threshold. Intensity is determined by dividing severity by duration, while inter-arrival time is the elapsed time (in months) between two consecutive drought events.

Figure 2. Illustration of drought categories (including No-Drought, Mild, Moderate, Severe, and Extreme) and drought events (frequency) and their characteristics (including severity, duration, and inter-arrival time) calculated using SPEI-12.

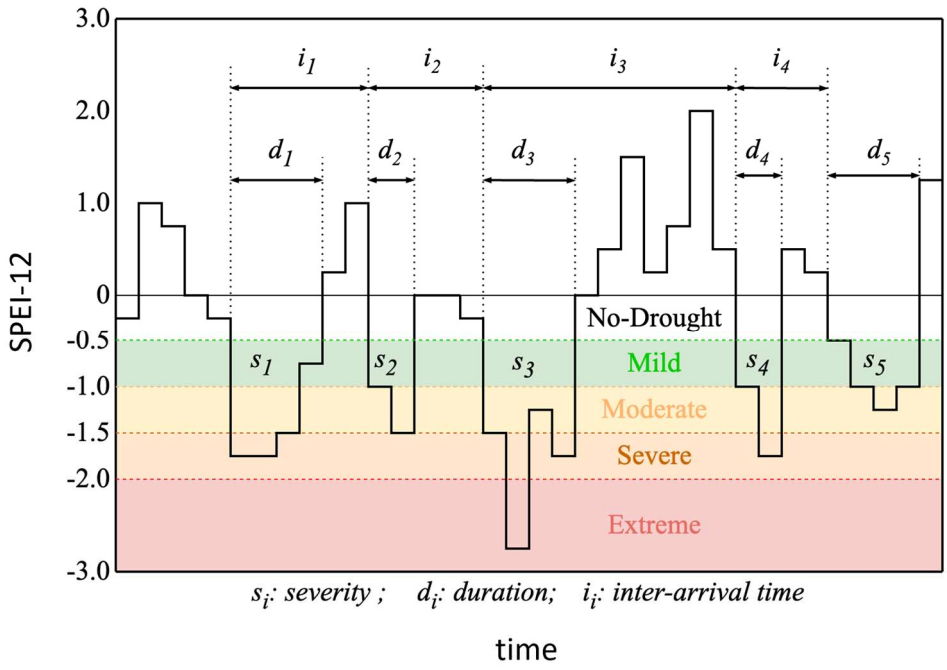

Source: Authors' own visualization. Original.

Given the coverage of the CMIP6-VN dataset for the historical (1980–2014) and future (2015–2099) periods, we selected the 30-year period of 1985–2014 as the reference period for fitting the probability distributions and estimating the parameters. The estimated parameters are then subsequently applied to the entire time series. This calculation procedure is recommended in several studies (e.g., Touma et al., 2015; Tam et al., 2023). It is worth noting that we also tested alternative methods, such as calculating SPEI separately for the reference and future periods or using a merged data series combining both periods. However, these approaches (not shown) yielded no significant differences in the results.

2.4. Bivariate joint distribution using copula

Given the stochastic and multifaceted nature of droughts, it is imperative to simultaneously assess multiple drought characteristics for an accurate assessment of drought risk. To model the relationship between drought characteristics, an effective approach is the utilization of bivariate joint distribution models. These models elucidate the relationship and distribution of two variables, providing insights into their joint behavior. However, developing these models can be challenging, as the distinct distributions of drought characteristics violate the requirement that all marginal distributions belong to the same family (Frees and Valdez, 1998). To address this issue, Shiau (2006) employed a copula-based technique (Sklar, 1959) to model the joint distribution of drought duration and severity. By separating dependence effects from marginal distribution effects, copula-based techniques have been widely applied in various drought-related studies (Shiau and Modarres, 2009; Kwon and Lall, 2016; Amirataee et al., 2018; Das et al., 2020; Li et al., 2020; Poonia et al., 2021). In this study, we employ copula-based techniques to compute the joint return period of drought severity and duration. The calculation process is structured into two phases: 1) identifying the univariate distribution functions of drought

severity and duration; and 2) applying copulas to combine the univariate distributions into a bivariate distribution.

Specifically, for each sub-climatic region, all drought events and their corresponding severity and duration are estimated using the aforementioned method (Figure 2). In the initial phase, four distributions, including "log-normal", "exponential", "gamma", and "Weibull", are fitted and evaluated to identify suitable parameters separately for severity and duration. The Akaike information criterion (AIC) (Akaike, 1974) and Bayesian information criterion (BIC) (Schwarz, 1978) are used to select the most appropriate distribution, while the Kolmogorov-Smirnov, Cramer-von Mises, and Anderson-Darling tests ensure goodness-of-fit at the 5% significance level. Based on our calculations, the "Weibull" distribution is the most prevalent for duration across the seven sub-climatic regions. Conversely, the "log-normal" distribution is more prevalent for severity data, followed by "exponential" and "Weibull" distributions.

In the subsequent phase, the most suitable copula is identified for each case by comparing the AICs of four representative copula functions (i.e., "Gaussian", "Clayton", "Frank", and "Gumbel"), fitted using maximum likelihood estimation. We observe that the "Frank" copula exhibits the highest dominance.

The joint return period, defined as the average elapsed time or mean inter-arrival time between occurrences of critical events, is estimated by calculating the probability that all values exceed specified thresholds. Specifically, the joint return period (T_{DS}) of a drought event with severity (S) and duration (D) exceeding specified thresholds (s) and (d), respectively, is calculated using the following equation (Shiau, 2006):

$$T_{DS} = \frac{E(L)}{P(D \geq d \ \& \ S \geq s)} = \frac{E(L)}{1 - F_D(d) - F_S(s) + F_{DS}(d,s)} = \frac{E(L)}{1 - F_D(d) - F_S(s) + C(F_D(d), F_S(s))} \quad (3)$$

where $E(L)$ represents the expected drought inter-arrival time, $F_D(d)$ and $F_S(s)$ are the cumulative distribution functions of D and S, respectively, and $F_{DS}(d, s)$ is the joint drought duration and severity distribution, which can be computed by the copula distribution function C.

2.5. Global warming level

The CMIP6 climate models include a new and improved representation of processes and a higher spatial resolution compared to the previous generation (CMIP5). However, they also show a broader range of equilibrium climate sensitivity (ECS). A subset of models have an ECS above the "likely" or even the "very likely" range assessed in the Sixth Assessment Report (AR6) of the Intergovernmental Panel on Climate Change (IPCC, 2021) based on multiple lines of evidence. These "hot" models simulate a warming rate higher than previously expected for a given scenario, which does not seem consistent with other lines of evidence. Therefore, using the ensemble mean of CMIP6 models for regional climate impact assessments may lead to an overestimation of the magnitude of change. To overcome this issue, Hausfather et al. (2022) recommend either basing climate analyses on global warming levels (GWLs) rather than on time or using the subset of models most consistent with the IPCC assessment of global climate sensitivity. This does not preclude considering high-sensitivity models to investigate tail-risks.

Therefore, in this study, we follow the new approach of IPCC AR6 and the recommendations of Hausfather et al. (2022) by complementing scenario-based analysis with projections based on GWLs. This approach is justified by the fact that for many climate variables, such as temperature and

precipitation, the patterns of future changes are strongly related to GWL but more or less independent of the pathway or the time at which the GWL is reached (IPCC, 2021).

GWLs 1°C, 1.5°C, 2°C, 3°C, and 4°C are defined when comparing global mean surface air temperature for a certain time in the future with that for the period 1850–1900. The GWL year is estimated for each GCM and SSP scenario. The period corresponding to a given GWL for each of the 22 CMIP6 GCMs used in this study is inherited from the results of Hauser et al. (2021). To minimize short-term variability, a 21-year window is employed, encompassing the initial year (Y_{GWL}) when the average temperature exceeds the threshold and 10 years preceding and following that year. Note that this 21-year window, chosen for better symmetry regarding Y_{GWL}, differs slightly from Hauser et al. (2021), who applied a 20-year window with 10 years preceding and 9 years following Y_{GWL}. The climatological values and the change between the future and baseline periods should be nearly identical for the 21-year and 20-year windows (not shown).

The climate response pattern for a specific GWL is determined as the average across all models and scenarios that reach that GWL. In our analysis, we provide a summary of the number of available models under each GWL and different scenarios in Table S1. For comparison purposes, we also include a "Baseline" with a 21-year period from 1994 to 2014 based on 22 reference simulations. However, we exclude cases where the first or last year of the 21-year period falls before or after 2015 or 2099 to avoid overlapping the Baseline with GWLs. Furthermore, as shown in Table S1, there are only two cases that meet GWL 1°C, so we exclude this GWL 1°C from our analysis.

3. Results

3.1. Changes in mean annual rainfall and temperatures

The ensemble mean patterns of the 22 models are examined for the reference period (1985–2014) and two future periods: the near future (2025–2054) and the far (or late) future (2070–2099), as illustrated in Figure 3. The model ensemble mean for the reference period exhibits strong agreement with observation data from the Vietnam Gridded Climate Dataset version 2 (VnGC) (Tran-Anh et al., 2023). This high level of agreement is attributed to the use of the BCSD downscaling technique in constructing CMIP6-VN, which incorporates bias correction based on the observational VnGC data (Tran-Anh et al., 2023).

For mean annual precipitation, the simulations across all periods exhibit a relatively consistent spatial distribution (Figure 3). The wettest regions are identified in R4 and R5, certain northern areas of R1 and R2, and parts of R6. In future periods, relative changes in precipitation vary by scenario. In the near future, most areas of Vietnam are projected to experience a slight increase (approximately 5% in most areas), except for some parts of the Central Highlands (R6) where changes are not statistically significant. In the far future, precipitation is projected to increase more significantly across the entire country (5-10% in most areas). Results for annual changes presented in Figure 4 further confirm these trends. Interestingly, while higher median values are projected under all scenarios (except in the near future for R5), the interquartile range and outliers remain rather similar across scenarios and periods. Statistical validation results (i.e., p-values less than 0.05, indicated as hatched areas in Figure 3) suggest substantial uncertainties in projections for R6 and certain areas within R1, R2, and R3. Overall, projections for both future periods indicate that rainfall will increase most significantly in regions R4, R5, and specific areas of R1, R2, and R3, with R4 and R5 exhibiting the highest degree of significance. Meanwhile, the Central Highlands (R6) exhibit minimum and insignificant changes in the near future but become wetter in the far future.

In terms of mean annual temperature, all projections for future periods indicate warmer conditions compared to the reference period, with changes being statistically significant (p-value reported from a t-test is less than 0.05) across all regions. While differences between scenarios remain modest in the near future, the far future exhibits significantly larger differences between scenarios. However, although the interquartile range is indeed modest (1–2°C) in the near future, some years may experience very high anomalies (>4°C in northern regions) that were not observed in the historical period. For the far future, the lowest temperature increase is projected under SSP1-2.6, while the highest is obtained under SSP5-8.5. Spatially, although the northern region typically has lower baseline temperatures, future temperature increases there are higher than in the southern region. Under both SSP2-4.5 and SSP5-8.5 scenarios, some models simulate some years with annual changes as high as 8°C. Similarly, higher-elevation areas such as R6 and the western parts of R4 and R6, which currently exhibit lower climatological means, are projected to experience excessively higher temperature increases compared to surrounding areas. Frequency distributions (Figure 4) further highlight disparities in warming magnitude towards the end of the century, with the highest under SSP5-8.5, followed by SSP2-4.5, and SSP1-2.6.

Here, we have provided a brief overview of the changes in rainfall and temperature, as a detailed analysis of these changes, along with related extremes, is presented in another study (Tran-Anh et al. 2024, submitted). The findings indicate that Vietnam is projected to experience alterations in both precipitation and temperature patterns. Temperature increases, particularly towards the end of the century, show a strong dependence on the selected scenario, highlighting the vulnerability of future conditions to emission pathways. While a slight increase in precipitation may lead to wetter conditions, the substantial rise in temperature could intensify evapotranspiration, potentially offsetting or even reversing the wetter effect in terms of impacts on soil moisture. Notably, the projected changes in precipitation patterns exhibit much larger uncertainty compared to temperature, underscoring the

necessity for a thorough investigation of the most severe scenarios, which is critical for formulating effective response and adaptation strategies to address future climate risks.

Figure 3. Spatial distribution of mean annual precipitation (mm/month) and temperature (°C) (1st and 3rd rows, respectively) and projected changes (2nd and 4th rows, respectively) compared to the reference period 1985–2014 in the near and far future under different SSP scenarios. Hatched areas in panels at the 2nd and 4th rows indicate regions where changes projected by the 22 models are statistically insignificant (i.e., the p-value reported from a t-test is greater than 0.05).

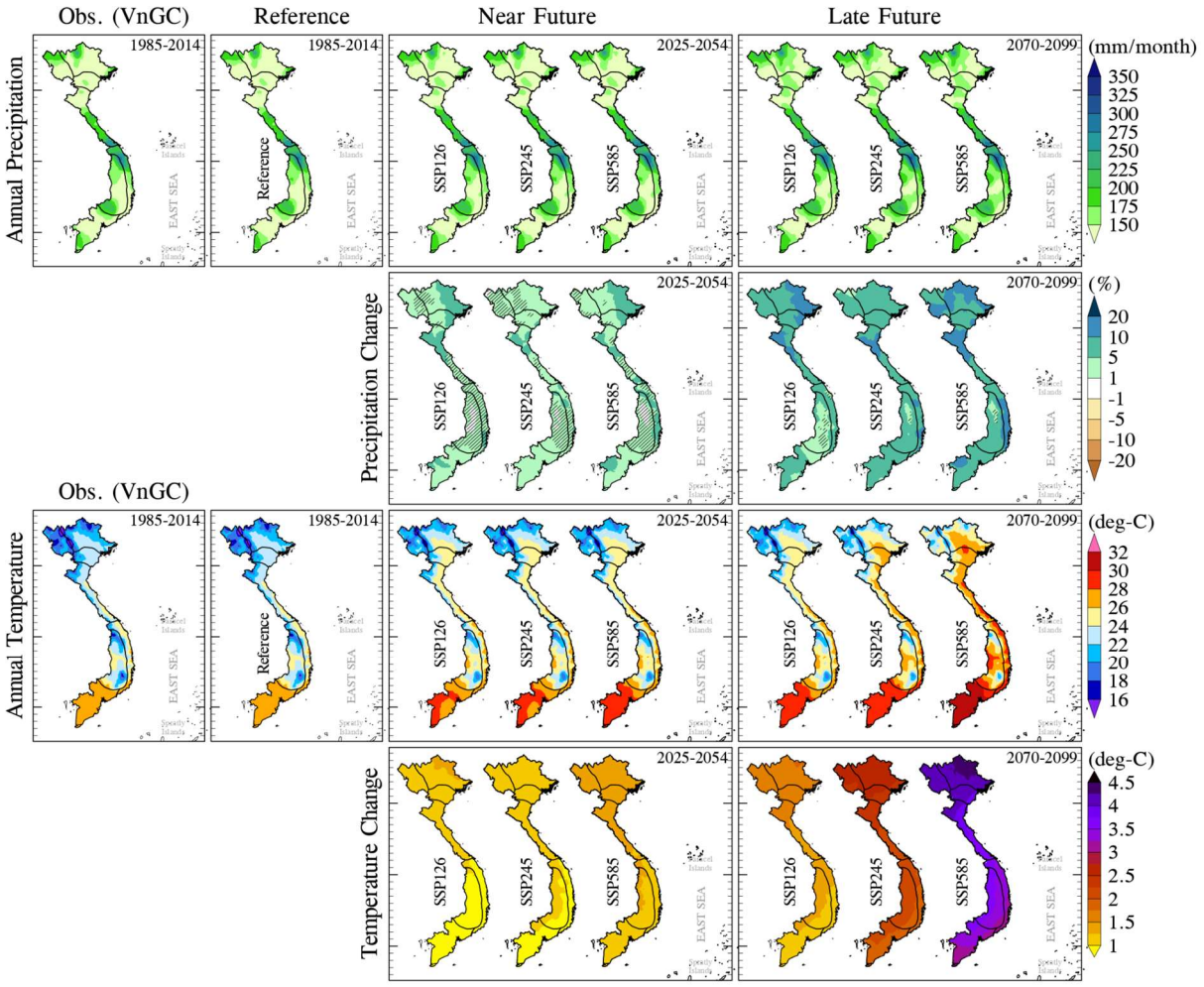

Source: Authors' own calculation. Original.

Figure 4. Boxplot illustrating the distribution of projected changes in (I) mean annual precipitation (%) and (II) mean annual temperature (°C) over the seven sub-climatic regions (a–g), as projected by 22 CMIP6-VN models. Results for the reference period (1985-2014) represent the biases between CMIP6-VN models and VnGC observations. Results for the near future period (2025–2054) and the far future period (2070–2099) under three distinct SSP scenarios illustrate changes relative to the reference period. The y-axis representing precipitation has been transformed using the "square root" function to enhance the visibility of low values.

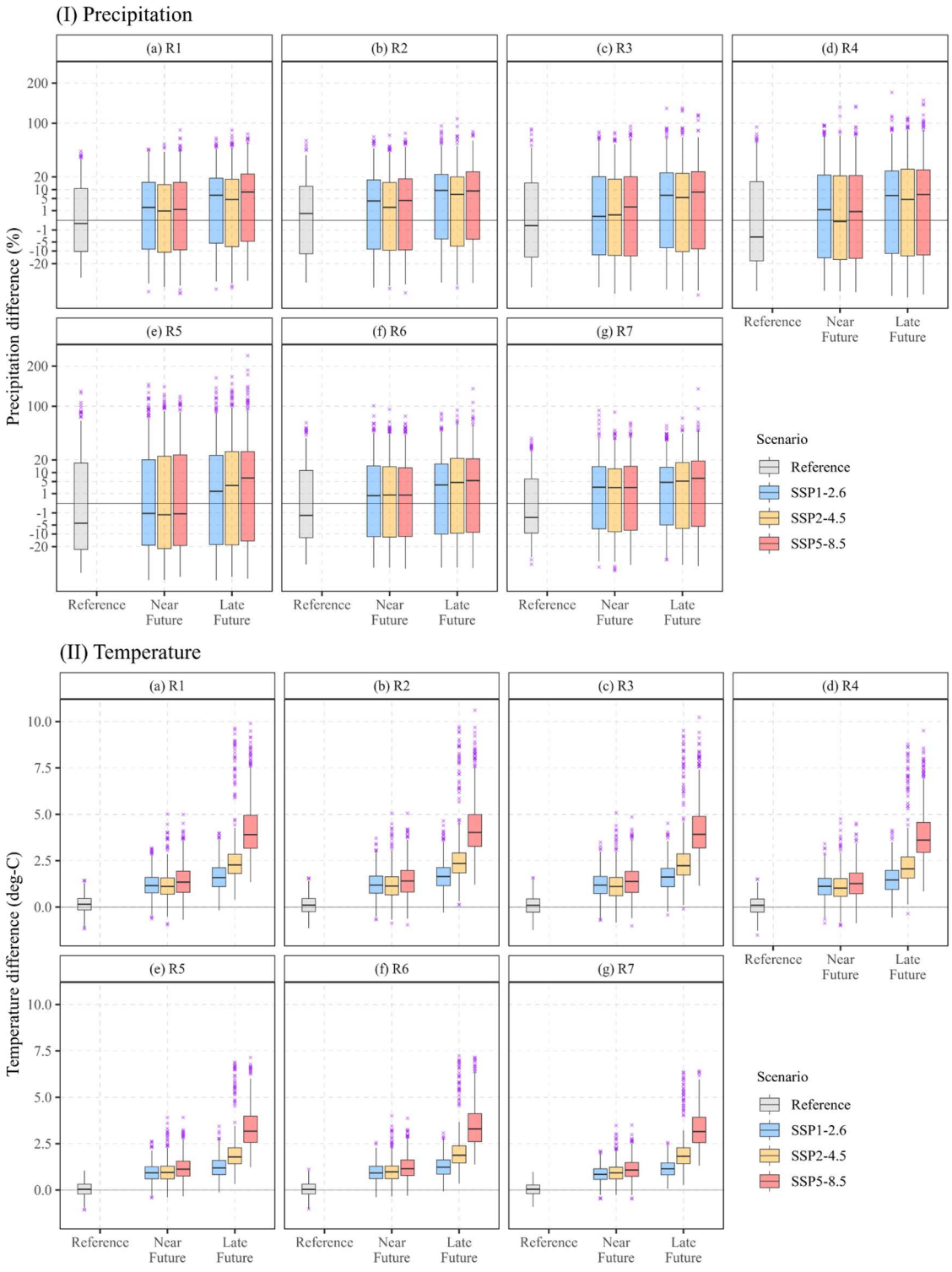

Source: Authors' own calculation. Original.

3.2. Drought projections from multi-model and multi-scenario experiments

3.2.1. Projected changes in drought conditions

Although the above analysis of the climatological mean of precipitation and temperature indicates that CMIP6-VN aligns well with observations, this does not necessarily imply that droughts calculated from this dataset will match observed droughts, due to the non-linear relationship between meteorological variables and drought characteristics (Droogers and Allen, 2002; Fu et al., 2023). Therefore, to assess the CMIP6-VN's capacity to represent droughts, we first compare the frequency density distributions (FDDs) of SPEI-12 obtained from the CMIP6-VN models with those of the VnGC data in the reference period (Figure 5). Across the seven sub-climatic regions, the results demonstrate that the FDDs of the CMIP6-VN models closely correspond to the observed SPEI-12. While some discrepancies exist among individual models at the peak of the bell curve, the ensemble mean of the 22 models' FDDs generally aligns with the observed SPEI-12.

Figure 5. Frequency density distribution of monthly SPEI-12 in the reference period (1985–2014) for each grid point within the 7 sub-climatic regions (a–g). The distributions are derived from the VnGC dataset (shaded area), individual CMIP6-VN models (thin black lines), and the ensemble of the 22 CMIP6-VN models (thick black line). Orange and blue shading indicates values below and above -0.5, representing dry and wet conditions, respectively.

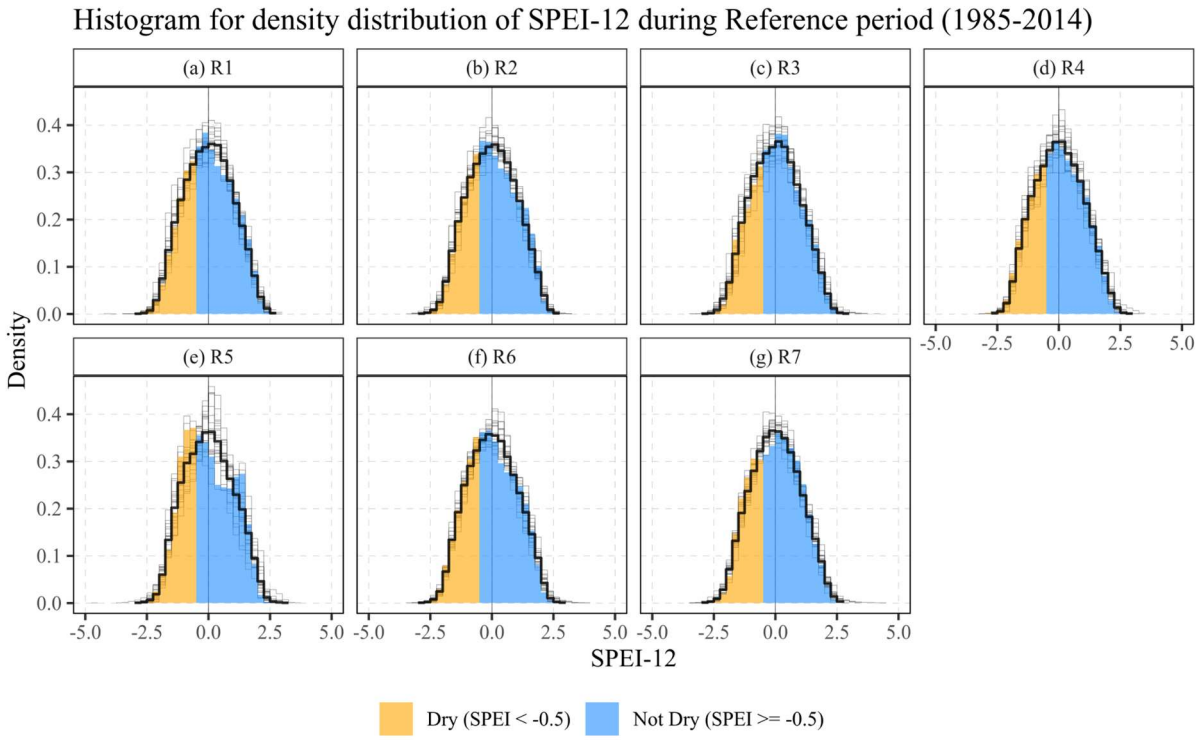

Source: Authors' own calculation. Original.

Similarly, we also examine the FDDs of SPEI-12 for the two future periods under the three scenarios in each of the seven sub-climatic regions (Figure 6). The ensemble results suggest a shift towards more positive SPEI-12 values in the future, indicating a tendency towards fewer drought events. However, the distribution for the future periods also shows longer tails, including instances extending towards more negative SPEI-12 values. This implies that while drought events may become less frequent, rare but extreme events with very high severity could occur. The variability in the frequency curves of individual models indicates the substantial uncertainty associated with drought projections. Among the 22

models, some still exhibit curves that clearly shift to the left, with the density peaks higher than in the reference period and located below -0.5 — the threshold for identifying a drought event. This implies that these models project more severe drought conditions in the future, especially under the SSP5-8.5 scenario (Figure 6-III).

The high number of downscaled products obtained through various combinations of GCMs and SSP scenarios used here highlights the large inter-model spread for SPEI-12 projections and hence their uncertainty. Thus, this demands an investigation of the future SPEI-12 time series for individual models. Figure 7 presents the Mann-Kendall Tau (τ) results (Mann, 1945; Kendall, 1948) for the SPEI-12 time series derived from each of the 22 selected CMIP6-VN models for each sub-climatic region under the three SSP scenarios. A positive (negative) τ value indicates an increasing (decreasing) trend in SPEI-12 values, suggesting wetter (drier) conditions towards the end of the century.

Under SSP1-2.6, most models, except GISS-E2-1-G, project positive τ values. In contrast, the "warmer" SSP scenarios (i.e., SSP2-4.5 and SSP5-8.5) generally result in more frequent drought occurrences over the century. For SSP2-4.5 and especially SSP5-8.5, a greater number of models show negative τ values. For example, only 4 models project negative τ values in R1 under SSP1-2.6, but 11 models do so under SPP2-4.5 and SSP5-8.5. Projections under SSP1-2.6 exhibit relatively high consistency among the 22 models, suggesting lower uncertainty. However, the uncertainty, i.e. inter-model spread, increases significantly for SSP2-4.5 and SSP5-8.5. This could be attributed to the greater projected temperature increases under these scenarios, which provide additional energy, leading to complex interactions and increased atmospheric instability. The parametrizations of the resulting severe weather phenomena, such as thunderstorms and hurricanes, differ among climate models, which may increase uncertainty.

On the other hand, comparative results also reveal variations across the seven sub-climatic regions. For the SSP1-2.6 scenario, the differences between regions are minimal, whereas for the other two "warmer" scenarios, the distinctions become more pronounced, underscoring the impact of higher temperature conditions on the uncertainty of results.

Figure 6. Frequency density distribution of monthly SPEI-12 in the near future period (2025–2054) (blue lines) and far future period (2070–2099) (red lines), calculated for each grid point in the seven sub-climatic regions (a–g). The distributions are derived from 22 CMIP6-VN models (thin lines) and the ensemble mean of the 22 CMIP6-VN models (thick lines). Observations from the reference period (1985–2014) are included for comparison (shaded area), with orange and blue shading indicating values below and above -0.5, representing dry and wet conditions, respectively.

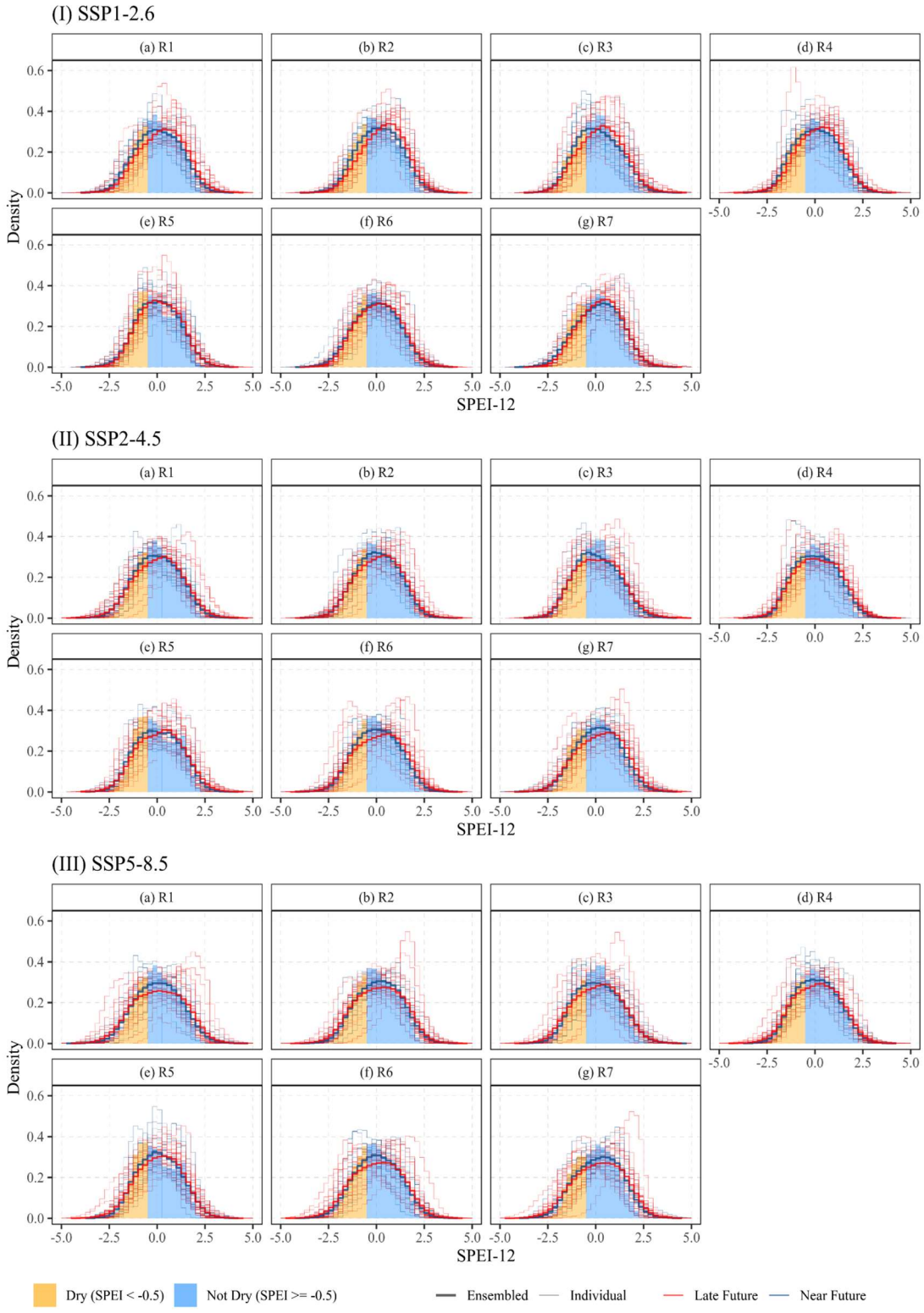

Source: Authors' own calculation. Original.

Figure 7. Mann Kendall's Tau (τ) values for area-averaged SPEI-12 across seven sub-climatic regions during the entire study period (1985–2099). These values are derived from the 22 CMIP6-VN models under three scenarios (top to bottom): SSP1-2.6, SSP2-4.5, and SSP5-8.5. Black-bold numbers indicate statistically significant values ($p < 0.05$), while gray numbers denote non-significant values ($p \geq 0.05$).

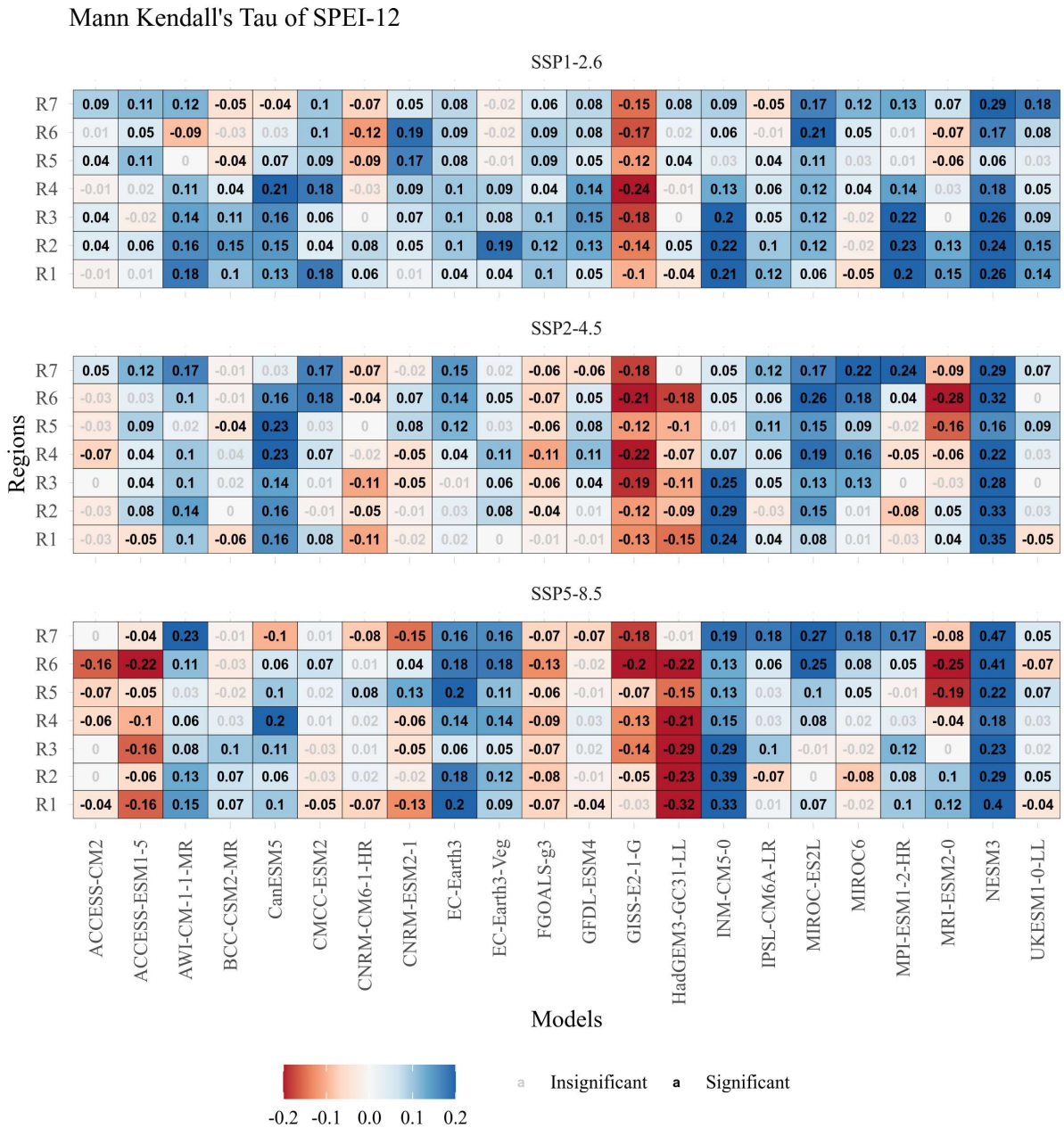

Source: Authors' own calculation. Original.

To verify the results of τ, time series of area-averaged SPEI-12 are extracted for each of the seven sub-climatic regions from CMIP6-VN models that perform well over Vietnam and exhibit the most pronounced differences, namely HadGEM3-GC31-LL (Figure S1) and EC-Earth3-Veg (Figure S2). Both original CMIP6 GCMs for these two selected products provide satisfactory results in representing rainfall and temperature over Vietnam, with their final-rank scores even surpassing the ensemble mean of all models (i.e., ENS-MEAN in Nguyen-Duy et al., 2023). The results from HadGEM3-GC31-LL

indicate a more pronounced trend of continuous drought occurrences across the century under SSP5-8.5, with some lasting up to several years in the second half of the century. In contrast, the results from EC-Earth3-GC31-LL suggest relatively wetter climate conditions in the second half of the century. However, the results from EC-Earth3-Veg reveal a considerable number of drought events in the mid-century compared to the end of the century. This implies that, although numerous models project a decreasing trend in drought towards the end of the century, earlier and mid-century periods may still experience frequent drought events.

Using the SPEI-12 values derived from each of the 22 CMIP6-VN models, drought events are identified, along with the distinctive characteristics of each individual case. Subsequently, the characteristics of drought events are aggregated from the 22 models for each scenario and presented in Figure 8. At the national scale, the geographical pattern of drought characteristics remains relatively consistent across the 3 SSP scenarios. In terms of frequency, the Central Highlands region (R6) and R1, R2, and R3 regions tend to experience more drought events compared to other regions. Notably, drought events in R6 are also more severe, characterized by higher severity, longer duration, slightly greater intensity, and shorter inter-arrival time. Furthermore, the intensity of drought in R6 also appears to be higher. It is worth reminding that the majority of projections for this region suggest limited precipitation increase, while temperature is unequivocally rising (Figure 3 and Figure 4). Conversely, the coastal areas of regions R4 and R5 will experience fewer droughts than the other regions. Furthermore, the time interval between consecutive droughts in these regions will be longer compared to the other regions. This is because these regions receive significantly more precipitation, as illustrated in Figure 3. On the other hand, northern Vietnam, encompassing regions R1, R2, R3, and the northern parts of R4, will experience more frequent droughts. However, the characteristics of these droughts are generally less severe than those in the Central Highlands. Even if there are differences in projected drought characteristics depending on the SSP scenario, there is a trend of increased severity and duration in some regions (R1, parts of R4, R5, and R6) in the warmer scenarios SSP2-4.5 and SSP5-5.8 compared to SSP1-2.6.

The aforementioned interpretations, once again, are based on the results ensembled from the 22 CMIP6-VN models. While this approach may potentially reduce the uncertainty associated with multiple model projections, it could also smooth out the signal and potentially lead to results favoring a more diminished representation of drought conditions—potentially hiding tail risks. Furthermore, it appears that future changes in precipitation and temperature exhibit no discernible relationship in both spatial and temporal patterns (Figure 3 and Figure 4). Similarly, the contribution of the two variables to the changing trend of SPEI-12 remains unclear, suggesting an investigation of their roles in drought projections to gain a better understanding of the future.

Figure 8. Spatial distribution of future drought characteristics (2015–2099) ensembled from the 22 CMIP6-VN models. The characteristics include (from left to right): frequency (i.e., number of drought events), as well as the climatological mean of severity, duration, intensity, and inter-arrival time of all drought events.

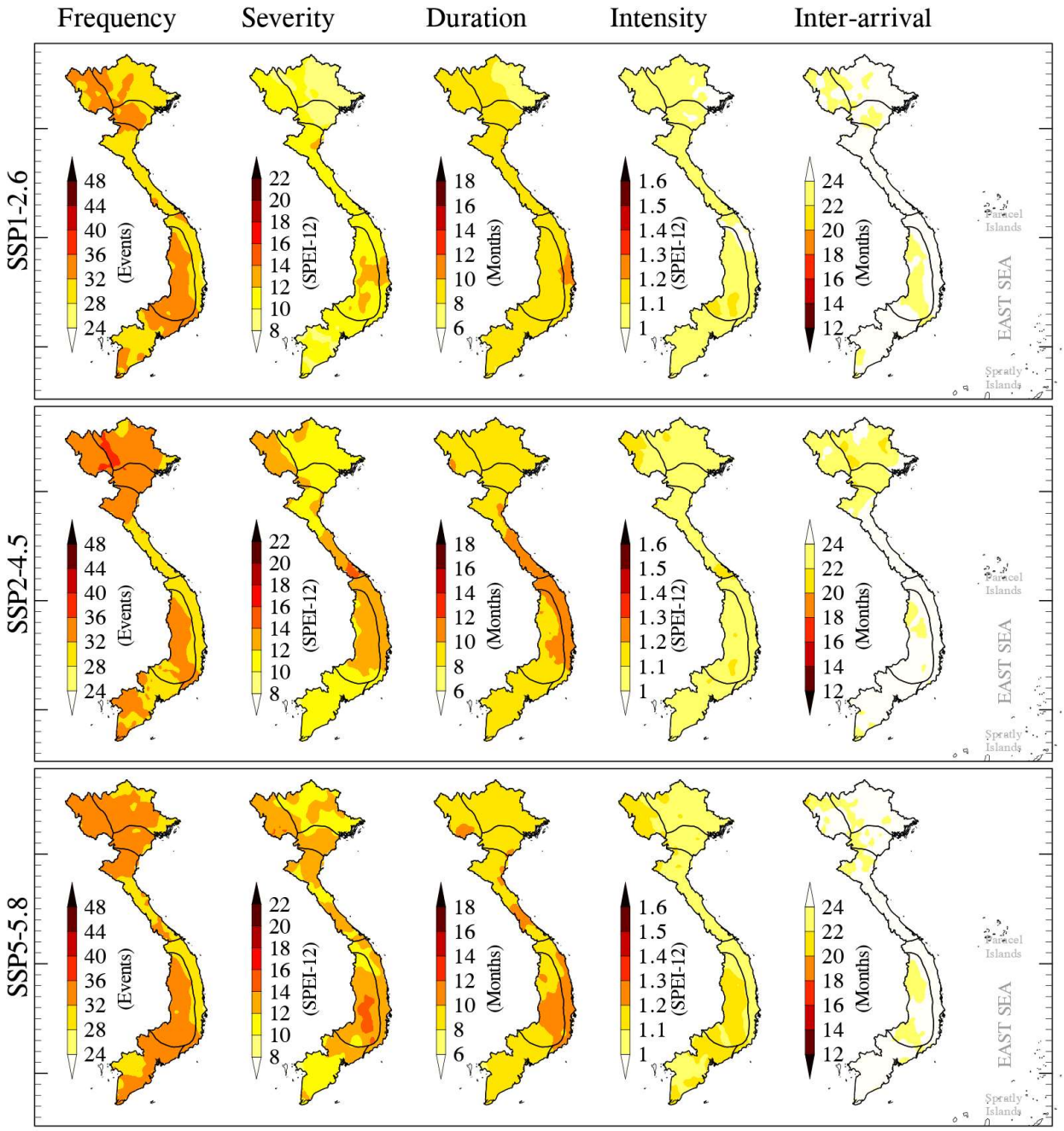

Source: Authors' own calculation. Original.

3.2.2. Roles of temperature and precipitation in drought projection results

The primary cause of drought has often been attributed to a deficiency of precipitation (Mckee et al., 1993). However, relying solely on precipitation to derive drought conditions may not yield proper results in certain regions where an increasing trend in precipitation has been widely reported, for instance, the Sahel, eastern Russia, North China, and northern high latitudes (Ukkola et al., 2020; Zhao and Dai,

2021), and even in Vietnam (as depicted in Figure 3). Several studies have underscored the pivotal role of temperature, as climate warming exponentially enhances potential evapotranspiration (Vicente-Serrano et al., 2010; Beguería et al., 2014; Vicente-Serrano et al., 2014; Fu et al., 2023). Notably, Fu et al. (2023) concluded that under global warming conditions, the impact of rising temperatures on intensifying drought may outweigh that of precipitation.

Consequently, in addition to the original experiment (referred to as "Original"), which utilized the original downscaled projections of precipitation and temperature, we designed two more experiments aimed at isolating the individual contributions of precipitation and temperatures to the future climatic water balance, CWB (Table 2). The "Detrended-Pr" and "Detrended-Tas" experiments retain the original temperature and precipitation values, respectively, but use the detrended and historicized versions of precipitation and temperature respectively. To achieve this, the time series of precipitation or temperature were first detrended using a least-square linear fit and then adjusted by the climatological mean of the reference period 1985–2014. The results of these "Detrended-*" experiments are illustrated in Figures 9 and 10, which further validate our assumptions.

Table 2. Experimental design for evaluating the roles of precipitation and temperature in the uncertainty of drought projection results.

Experiment	**Data for SPEI-12 calculation**	
	Precipitation (Pr)	**Air Temperature (Tas)**
Original	Original	Original
Detrended-Pr	[Detrended Pr] & [Reference's Climatology]	Original
Detrended-Tas	Original	[Detrended Tas] & [Reference's Climatology]

In comparison to the "Original" presented in Figure 7, the results of the Mann-Kendall Tau (τ) statistic presented in Figure 9 clearly demonstrate the role of precipitation and temperature on the evolving trend of SPEI-12 across the century. Both new experiments significantly alter drought conditions, resulting in distinctly drier or wetter conditions in almost all scenarios. When the increasing trend of temperature is removed in the "Detrended-Tas" experiment, the PET is anticipated to be lower than in the original experiment, leading to wetter conditions (i.e., a positive τ, indicating an increase in SPEI-12). Conversely, when the increasing trend of precipitation is removed in the "Detrended-Pr" experiment, water resource scarcity is anticipated to result in drier conditions (i.e., a negative τ, indicating a decrease in SPEI-12).

Figure 10 presents an analysis of the contributions of precipitation and temperature to the SPEI-12 results for each of the seven sub-climatic regions. Specifically, Figure 10-I employs combined box- and violin plots to illustrate the distributions of yearly differences in area-average SPEI-12 between the "Detrended" and "Original" experiments (i.e., "Detrended" minus "Original") during the near future (2025–2054) and the far future (2070–2099) under three SSP scenarios. All cases demonstrate the distinction in the impacts of precipitation and temperature on SPEI-12. When the two sections — "blue-shaded" (representing the contribution of precipitation) and "orange-shaded" (representing the contribution of temperature) — are distinctly separated at the zero axis, it becomes evident that the discrepancies between the two experiments are greater in the far future compared to the near future. This is because

changes in both precipitation and temperature exhibit stronger tendencies towards the end of the century, as discussed in Section 3.1.

Furthermore, in almost all cases, the absolute magnitude of "Detrended-Pr" is significantly higher than that of "Detrended-Tas", indicating that precipitation contributes more to the calculation of SPEI-12. Additionally, the distributions of differences between "Detrended-Pr" and "Original" are spread over a wider range of values compared to those of "Detrended-Tas". This could be attributed to the large spread in temperature projection results, with high temperature outliers (Figure 4(II)), which are no longer offset by rising precipitation in Detrended-Pr. When comparing SSP scenarios, SSP5-8.5 clearly exhibits the largest discrepancies between the two experiments. In the "Detrended-Pr" experiments, the differences with "Original" seem to have more outliers, with many cases being located significantly far from the main boxes. This, again, could be attributed to temperature outliers that are no longer compensated by rising precipitation in Detrended-Pr.

To approximately quantify the contributions of precipitation and temperature trends to the SPEI-12 results, we calculate the percentage of their impacts by dividing the absolute difference between the "Detrended" case and the "Original" by the total sum of the absolute differences between both "Detrended-*" cases and the "Original". The results for each sub-climatic region under each SPP scenario are illustrated in Figure 10-II, demonstrating that the contribution of precipitation to drought results is significantly higher than that of temperature. In almost all cases, the impact of increasing temperature on SPEI-12 trends is relatively minor, ranging from about 5 to 15%. However, the influence of temperature appears to increase toward the end of the century, with its effect becoming more pronounced under the "warmer" scenarios. In the far future under SSP5-8.5, where temperature is projected to increase significantly across the entire country, temperature trends account for approximately 30% of the SPEI-12 trend results.

Figure 9. Similar to Figure 7, but for the "Detrended-Tas" experiment (panel I) and the "Detrended-Pr" experiment (panel II).

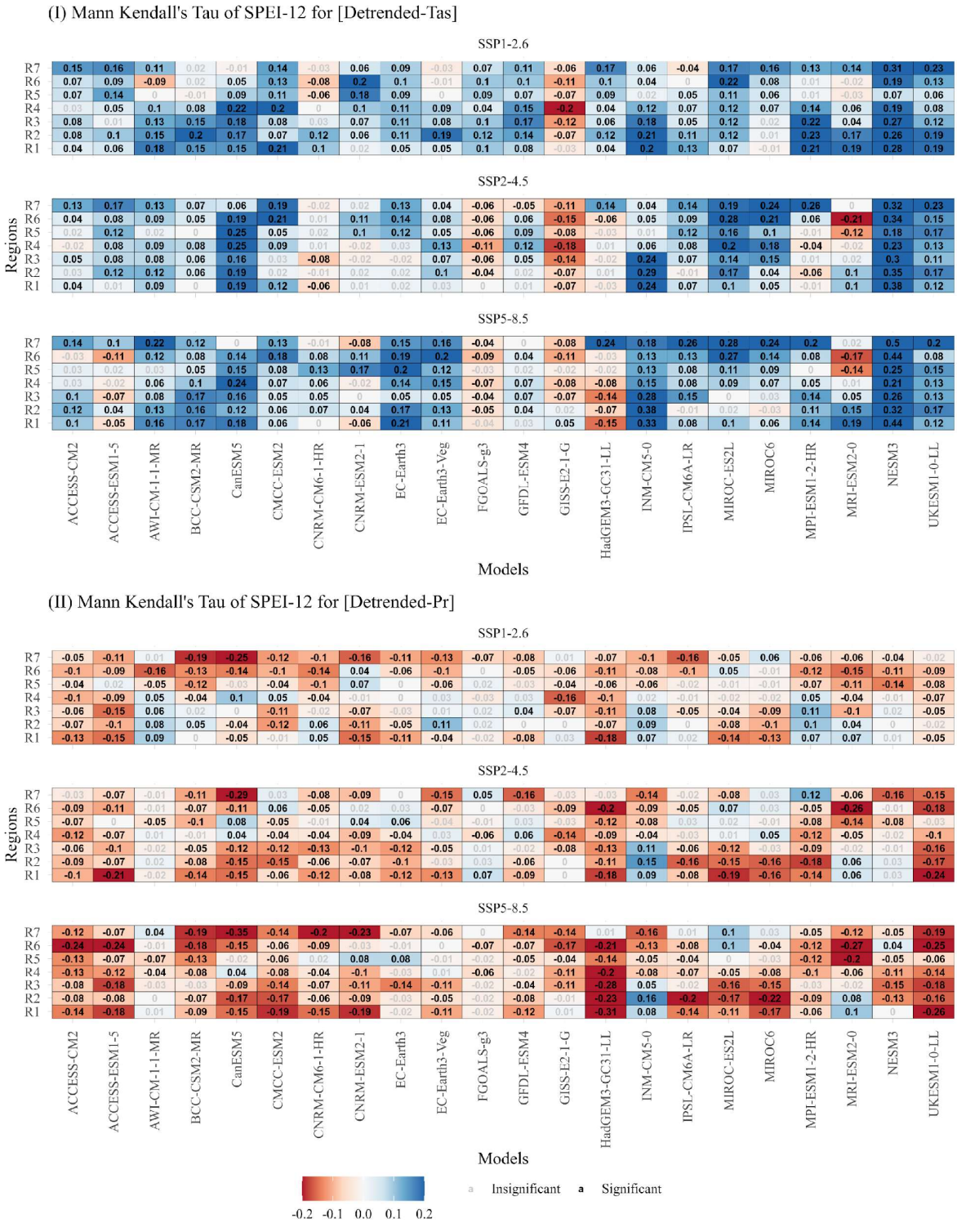

Source: Authors' own calculation. Original.

Figure 10. Comparison of the "Detrended" experiments, including: (I) distributions of yearly differences in area-averaged SPEI-12 between the "Detrended" and "Original" experiments ("Detrended" minus "Original") in the 7 sub-climatic regions, calculated using 22 CMIP6-VN models for near future (2025–2054) and far future (2070–2099) under 3 SSP scenarios; and (II) Estimation of the relative impacts of precipitation (blue shaded) and temperature (orange shaded) on future drought calculation for each of the 7 sub-climatic regions during different future period under 3 SSP scenarios. The numbers in blue/orange zones of panel II presents the average percentage of impacts of precipitation/temperature across the 7 sub-climatic regions.

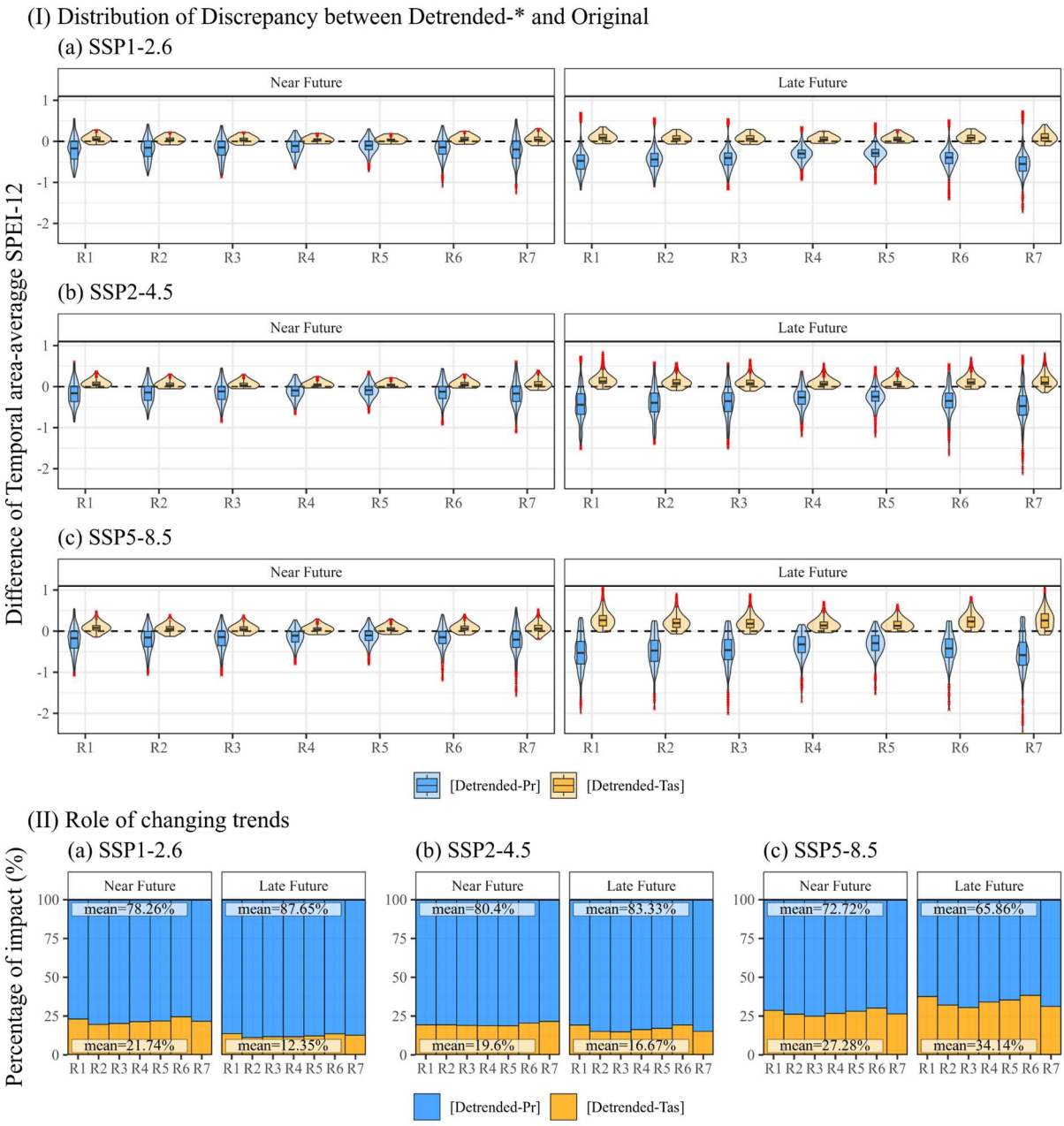

Source: Authors' own calculation. Original.

3.3. Drought conditions under different Global Warming Levels

To compare drought conditions between specific GWLs and Baseline, we perform a statistical analysis of common metrics and the distribution of SPEI-12 values over a 21-year period, with each year including twelve 12-month accumulated values of SPEI-12. The results of this analysis are firstly illustrated via the box- and violin plots in Figure 11. Overall, the seven sub-climatic regions exhibit remarkably similar patterns. Datasets of SPEI-12 estimated from the Baseline period have box- and violin-shaped distributions that are quite similar to GWLs 2°C or 3°C, depending on the region. As GWLs increase, the distribution of SPEI-12 values becomes more dispersed, manifesting in a substantial range between Q25 and Q75 (i.e., the interquartile range) and the presence of additional outliers. This indicates that while the overall patterns of drought may not exhibit significant differences, there is a possibility of an increased frequency of extreme drought events with higher GWLs.

The investigation of drought characteristics during the 21-year period of the Baseline and GWLs depicted in Figure 12 further supports the aforementioned assumption. Note that the differences between GWLs and the Baseline have been tested for statistical significance using both a t-test and the bootstrap technique (Efron and Tibshirani, 1993), with results from both methods closely matching (Figure 12 for the t-test and Figure S3 for the bootstrap results). Characteristics of droughts estimated for GWLs 1.5°C and 2°C are quite similar and closely resemble the Baseline. The intensity of drought events in these GWLs is slightly higher than the Baseline, while the inter-arrival time of drought events appears to be longer. For GWL 3°C, the frequency of droughts is comparable to the Baseline period. However, all other characteristics appear to be more severe than those of the Baseline. Although the frequency of droughts for GWL 4°C can be lower than that of other GWLs and the Baseline, the other characteristics clearly indicate that this GWL is expected to experience the most severe droughts.

Figure 11. Box- and Violin-plot for statistics and distribution of SPEI-12 area-averaged for each climatic region during the 21-year period of Baseline and different Global Warming Levels (GWLs), for all climate models and scenarios.

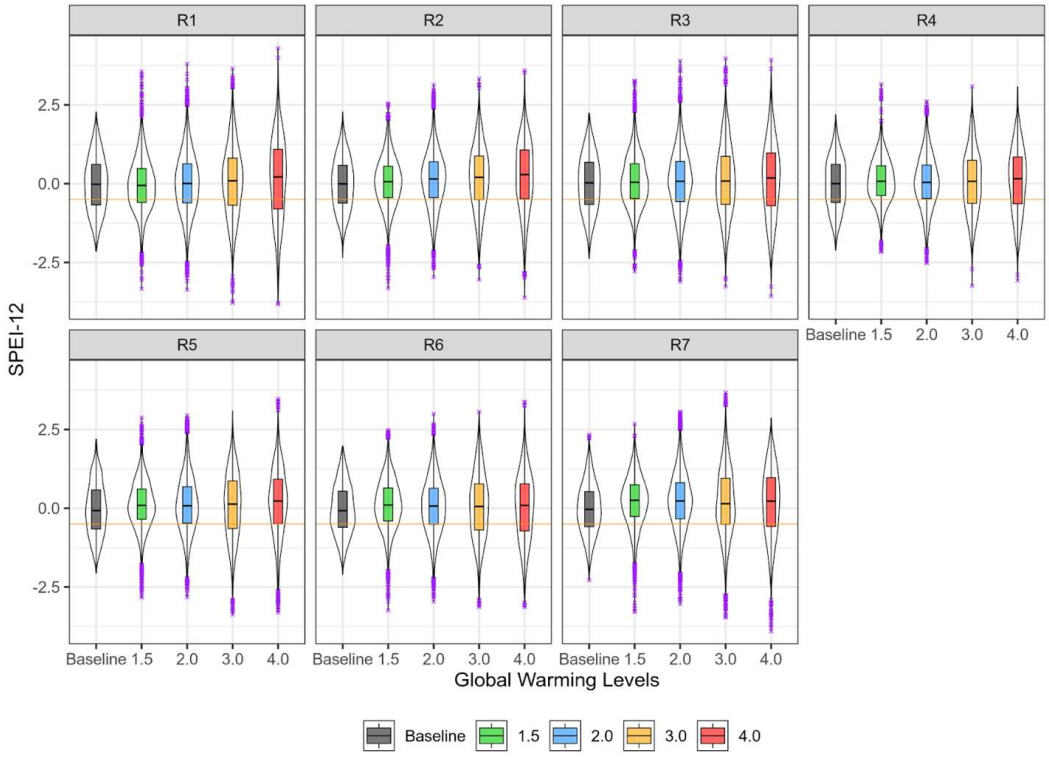

Source: Authors' own calculation. Original.

Figure 12. Spatial distribution of drought characteristics ensembled from the available models of the 21-year period of Baseline and the differences between GWL results with the baseline period. The characteristics include (from left to right): frequency (i.e., total number of droughts during the 21-year period), as well as the climatological mean of severity, duration, intensity, and inter-arrival time of all drought events. For the differences values, hatched areas indicate regions where changes are statistically insignificant (i.e., the p-value reported from a t-test is greater than 0.05).

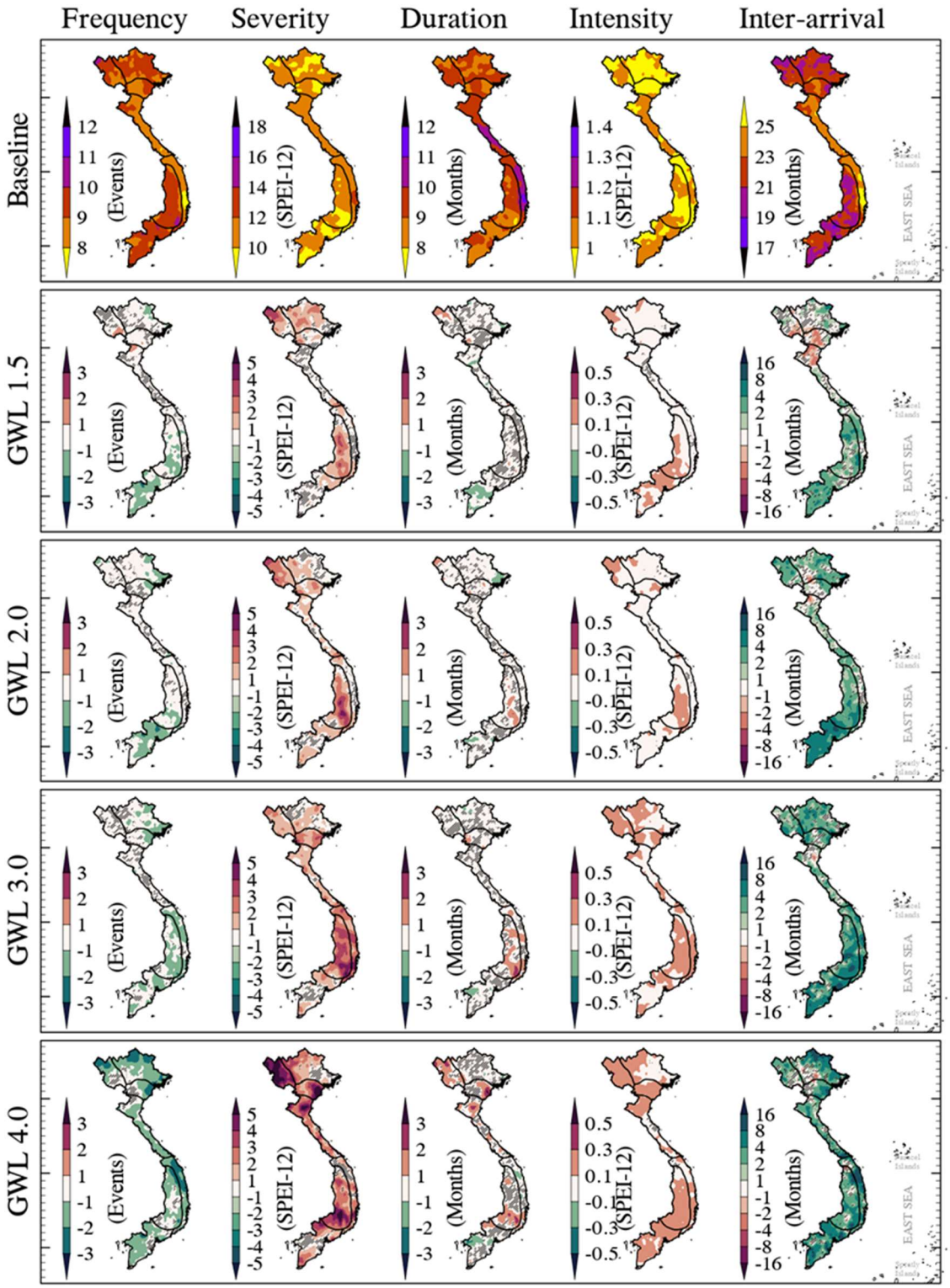

Source: Authors' own calculation. Original.

3.4. Future drought emergencies under the most severe projections

The previous sections highlight a substantial level of uncertainty in the SPEI-12 results among the CMIP6-VN models, with a major contribution from precipitation-related uncertainty. To prepare for the most severe climate change scenarios in terms of droughts in Vietnam, this section selects the CMIP6-VN models that exhibit the most pronounced increasing trend in drought (based on the Mann-Kendall's Tau values in Figure 7) to explore specific characteristics of droughts under these worst case scenarios. Through the analysis, five models have been chosen: HadGEM3-GC31-LL, GISS-E2-1-G, FGOALS-g3, CNRM-ESM2-1, and ACCESS-ESM1-5. It is worth noting that, in addition to projecting an increasing trend in drought toward the end of the century, these selected models also demonstrate relatively good simulation capabilities for the historical period for Vietnam, as evidenced by their high rankings in Nguyen-Duy et al. (2023).

Figure 11 illustrates the spatial distribution of drought event characteristics under different scenarios. To facilitate qualitative comparison, the color scales of Figure 13 are maintained in accordance with those of Figure 8. It is evident that the results from the five selected models are significantly more severe than the ensemble of 22 models. In the most severe case, drought events appear to occur approximately 1.5 to 2 times more frequently, exhibiting higher severity and longer duration. Furthermore, the intensity and inter-arrival time also exhibit a tendency toward worsening.

As the "warmth" of scenarios increases, the severity of drought events tends to intensify, and SSP5-8.5 exhibits the most extreme results. In terms of frequency, the Northern region (i.e., R1–3), Central Highlands (i.e., R6), and Southern region (i.e., R7) exhibit a distinct pattern, experiencing a higher number of drought events. Additionally, the severity and duration of droughts are also more pronounced in these regions. The average intensity of drought events reveals that regions R1, R6, and the northern part of R7 are projected to face more intense droughts in the future, particularly under the most severe scenarios. Regarding the inter-arrival time, higher SSP scenarios result in shorter intervals, which aligns with the increased frequency of consecutive events. In contrast, the Central and Coastal regions of Vietnam are projected to experience less severe future drought conditions compared to other regions. This could be attributed to the fact that the future precipitation projections consistently indicate a substantial increase in rainfall in these areas.

Figure 13. Spatial distribution of future drought characteristics (2015–2099) ensembled from the 5 most severe CMIP6-VN models (i.e., HadGEM3-GC31-LL, GISS-E2-1-G, FGOALS-g3, CNRM-ESM2-1, ACCESS-ESM1-5). The characteristics include (from left to right): frequency (i.e., number of drought events), as well as climatological mean of severity, duration, intensity, and inter-arrival time of all drought events.

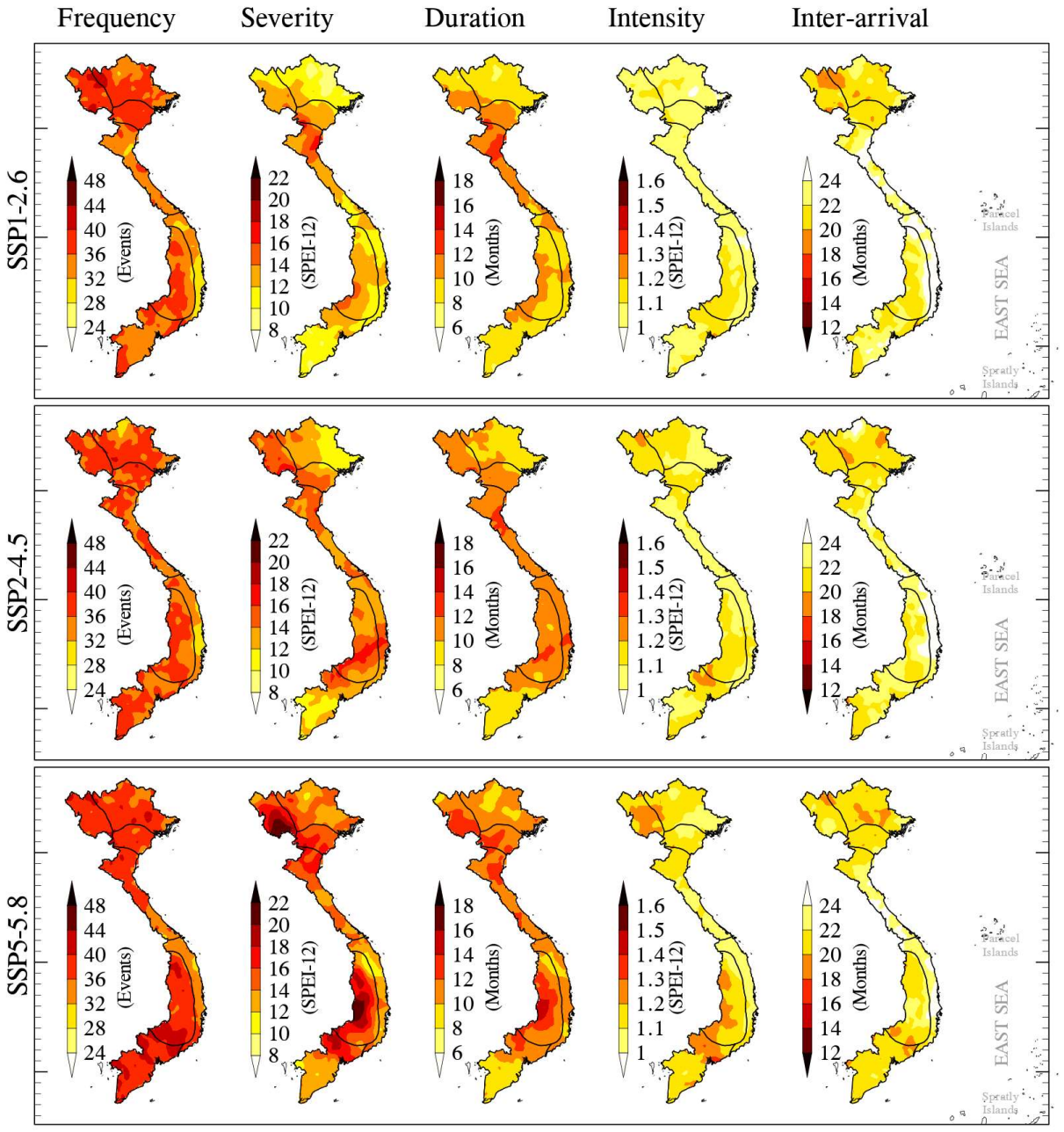

Source: Authors' own calculation. Original.

Utilizing the methodology outlined in Section 2.4, we construct bivariate joint distributions employing copulas to estimate the joint distribution of drought duration and severity. The results are presented in Figure 14, with overlaying lines indicating the return periods at 5 years, 10 years, and 50 years for each sub-climatic region under the 3 SSP scenarios. This visualization shows the disparities among the scenarios in most sub-climatic regions. In general, events with higher return periods tend to appear with longer durations and greater severity. In most cases, the "warmer" SSP scenarios tend to experience more severe droughts (including both extended duration and greater severity), with the exception of R4, where the differences between scenarios are minimal. Regions such as R1, R3, and R6 exhibit the most severe and prolonged drought events at all return period levels, with distinct differences between scenarios. Region R6 is particularly susceptible to experiencing the most severe drought conditions in terms of both severity and duration. Under the most severe scenario of SSP5-8.5, a 50-year return period drought can accumulate an absolute SPEI-12 value of 60 over a 31-month period. The region has a very high probability of experiencing extreme drought events.

Figure 14 also illustrates that during the Reference period (1985–2014), both observations and the modeled drought events exhibit a striking similarity. Statistically, the ensemble of all drought events (circle points) during the Reference period in both cases (green- and purple-circle points) exhibits severity and duration characteristics equivalent to events with a return period of approximately 5 years. Meanwhile, the extreme drought events (i.e., events with either duration or severity greater than the 95th quantile) (green- and purple-triangle points) correspond to return periods of approximately 10 to 15 years, indicating their rarity and greater intensity compared to average events. For better clarity, this interpretation can be expressed as follows: a drought event with a duration and severity comparable to the 5-year/10-year return period line has approximately a 20%/10% probability of occurrence, respectively.

For results under different SSP scenarios, the mean of all events during the period 2015–2099 exhibits characteristics of drought severity and duration that are predominantly located between the lines for return periods from 5 years to 10 years. Given that the length of the future period is significantly larger than that of the reference period (85 years vs. 30 years), it is possible that the results for the future period may be slightly underestimated, as the average potentially smoothes out the results. In all regions, larger changes are projected for extreme drought events. The duration of extreme events (>95th quantile) is projected to increase from approximately 15 months to around 30 months, while severity, quantified by the total absolute SPEI-12 values for each event, is projected to rise from about 20 to 40–50 depending on the region. Nevertheless, it is crucial to recognize that, in certain regions, such as R1, R3, and especially R6, some unprecedentedly severe droughts are likely to emerge in extreme cases under SSP2-4.5 and SSP5-8.5 (orange- and red-triangle points), exhibiting characteristics equivalent or surpassing those of an event with a return period of 50 years, meaning approximately a 2% probability of occurrence.

Figure 14. Bivariate joint return periods at 5-year (dotted lines), 10-year (dashed lines), and 50-year (solid lines) levels estimated from 5 most severe (denoted as 5-driest) CMIP-VN models for the entire future period (2015–2099) based on area-averaged drought duration (unit: months) and severity (sum of absolute SPEI-12 values during each event) for each of the 7 sub-climatic regions under the scenarios of SSP1-2.6 (blue lines), SSP2-4.5 (orange lines), and SSP5-8.5 (red lines). Circle markers represent the mean of all events, calculated from either Observations or the 5-driest CMIP6-VN models under the different scenarios (1985–2014 for Reference, and 2015–2099 for the SSP scenarios), while the triangle markers represent the means of all extreme events (i.e., events with either duration or severity greater than the 95th quantile). The colors of the markers are described in the legend.

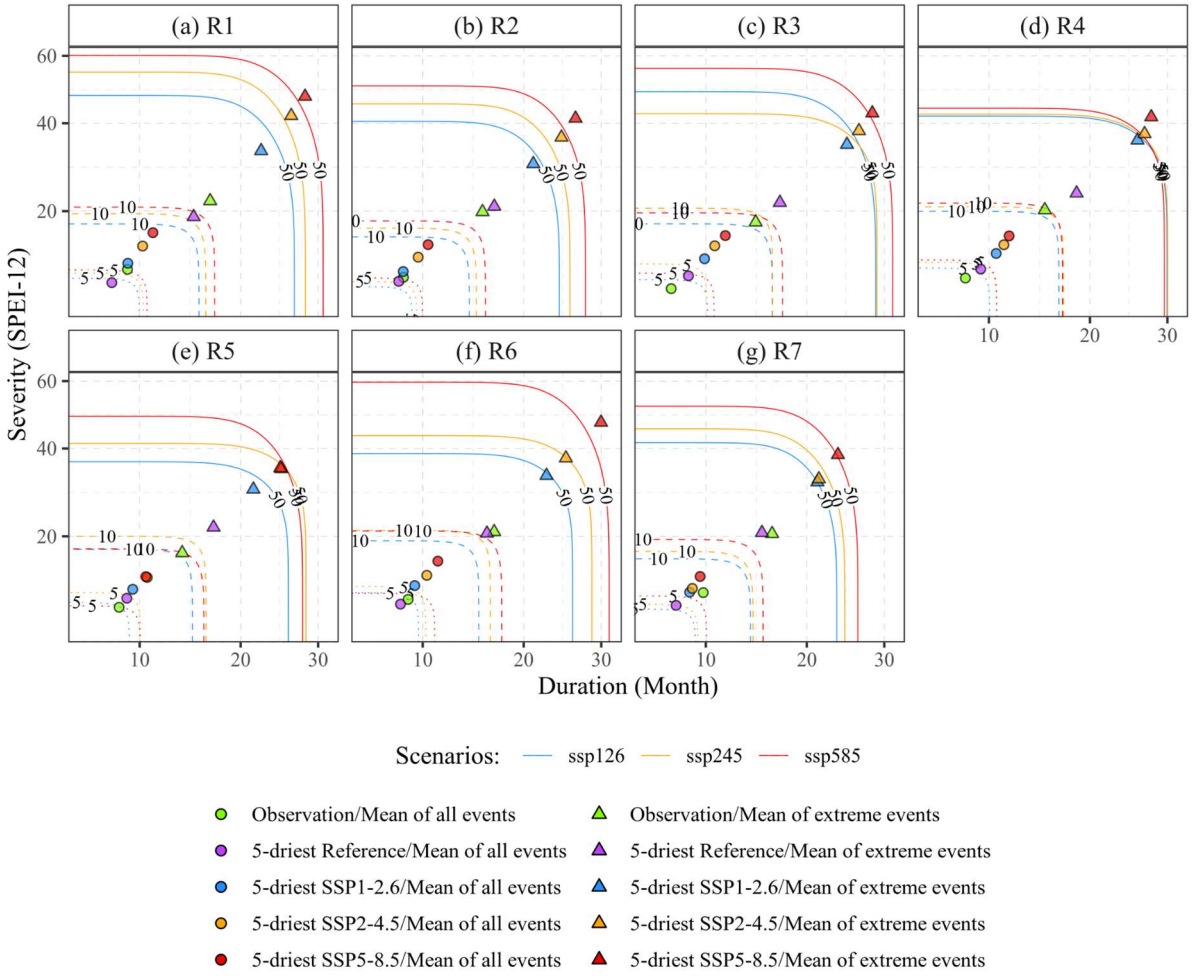

Source: Authors' own calculation. Original.

4. Conclusions

In this study, we employed the most up-to-date high-resolution downscaling products from 22 CMIP6 GCMs, known as the CMIP6-VN dataset, to investigate drought conditions over the seven sub-climatic regions of Vietnam. Daily data of precipitation and temperatures at a 10-km resolution from CMIP6-VN were utilized to calculate the Standardized Precipitation-Evapotranspiration Index (SPEI), a drought index that incorporates the effects of both precipitation and temperature-induced evapotranspiration. Our investigation was divided into three main parts, with key findings summarized as follows:

1) First, we explored the ability of CMIP6-VN to represent precipitation and temperature for the reference period (1985–2014) and the future period (2015–2099). The CMIP6-VN dataset can well capture the major characteristics of these variables in Vietnam. While temperature is projected to increase significantly across the country under all climate scenarios, with higher levels of warming for higher GLWs and high statistical significance, changes in precipitation remain uncertain, due to the large inter-model spread, although a general trend toward wetter conditions is projected. We subsequently discussed that, due to the large inter-model spread in the projections from multiple CMIP6-VN models, simple climatological means or ensemble approaches may obscure important drought signals and their associated risks, especially in the Central Highlands (R6).

2) Given that both temperature and precipitation contribute to the calculation of SPEI-12, we conducted two additional experiments to assess their respective impacts on drought estimation. This analysis aimed to determine the extent to which the uncertainty in precipitation projections influences drought conditions. The results demonstrate that precipitation has a significantly greater impact on the results of drought than temperature. Even in the most "warming" scenario, where temperature is projected to rise significantly toward the end of the century, precipitation still accounts for approximately 70% of the trend in SPEI-12. Nevertheless, temperature remains a significant factor in drought estimation, and failing to account for it would lead to an underestimation of future drought conditions.

3) Drought conditions under the different GWLs 1.5°C, 2°C, 3°C, and 4 °C were investigated, showing that while drought may not occur more frequently at high GWLs, their severity and intensity would increase, especially in the North regions and the Central Highlands.

4) Given the large inter-model spread associated with ensemble projections of drought, we selected five models that perform well over Vietnam and exhibit the most severe drought trends to further investigate worst-case scenarios. Even in this case, both the climatological mean of all drought events and the mean of extreme drought events show high agreement between observations and simulations of the 5 models during the reference period. Future projections indicate increased severity, duration, and intensity, particularly in regions R1, R2, and R6. In all regions and scenarios, large increases in the severity and duration of extreme events are projected. It is noteworthy that while the reference period can experience extreme drought events comparable to those with a return period of 10 years, the future period may be more hazardous, potentially experiencing events equivalent to those at a return period of 50 years.

Overall, in this study, we have developed a comprehensive and systematic approach to quantify the risks of drought events in Vietnam. While future drought characteristics remain highly uncertain across all climate scenarios due to significant inter-model spread, a key finding emerges: despite a general trend toward slightly wetter conditions, more severe—though not necessarily more frequent—drought events are projected. Some models even indicate the potential for prolonged and intense droughts, particularly under high warming levels. This finding presents a significant challenge for adaptation policy planning. Further action and research are essential not only to narrow the range of uncertainty but also to provide policymakers with the tools to develop targeted and flexible adaptation strategies. These strategies must align with the level of risk that society is willing to cope with and able to prepare for.

From a technical perspective, the use of dynamical downscaling, such as the efforts undertaken by the Coordinated Regional Downscaling Experiment - Southeast Asia (CORDEX-SEA) (Tangang et al. 2020; Ngo-Duc et al. 2024) could be considered to further address uncertainty and refine the understanding of drought patterns under future climate scenarios. Integrating such an approach would be a crucial step toward enhancing confidence in drought projections and supporting more informed decision-making in Vietnam.

Bibliography

AghaKouchak, A., Cheng, L., Mazdiyasni, O., & Farahmand, A. (2014). Global warming and changes in risk of concurrent climate extremes: Insights from the 2014 California drought. *Geophysical Research Letters*, 41(24), 8847-8852.

Akaike, H. (1974). A new look at the statistical model identification. *IEEE transactions on automatic control*, 19(6), 716-723.

Allen, R., Pereira L., Raes D., et al. (1998). Crop Evapotranspiration - Guidelines for Computing Crop Water Requirements - *FAO Irrigation and Drainage Paper 56*. FAO. 1998; Paper 56. Rome. p. 6541.

Amirataee, B., Montaseri, M., & Rezaie, H. (2018). Regional analysis and derivation of copula-based drought Severity-Area-Frequency curve in Lake Urmia basin, Iran. *Journal of Environmental Management*, 206, 134-144.

Arnell, N. W., & Gosling, S. N. (2016). The impacts of climate change on river flood risk at the global scale. *Climatic Change*, 134(3), 387–401.

Beguería, S., Vicente-Serrano, S. M., Reig, F., & Latorre, B. (2014). Standardized precipitation evapotranspiration index (Spei) revisited: Parameter fitting, evapotranspiration models, tools, datasets and drought monitoring. *International Journal of Climatology*, 34(10), 3001–3023.

Byun, H. R., & Wilhite, D. A. (1999). Objective quantification of drought severity and duration. *Journal of climate*, 12(9), 2747-2756.

Cook, B. I., Smerdon, J. E., Seager, R., & Coats, S. (2014). Global warming and 21st century drying. *Climate Dynamics*, 43(9–10), 2607–2627.

Dai, A. (2011). Drought under global warming: A review. *WIREs Climate Change*, 2(1), 45–65.

Dao, T. A., & Nguyen, N. M. (2022). Toward a sustainable food system and agroecology transition in Vietnam. *The VMOST Journal of Social Sciences and Humanities*, 64(1), 67-84.

Das, J., Jha, S., & Goyal, M. K. (2020). Non-stationary and copula-based approach to assess the drought characteristics encompassing climate indices over the Himalayan states in India. *Journal of Hydrology*, 580, 124356.

Diffenbaugh, N. S., Swain, D. L., & Touma, D. (2015). Anthropogenic warming has increased drought risk in California. *Proceedings of the National Academy of Sciences*, 112(13), 3931-3936.

Droogers, P., & Allen, R. G. (2002). Estimating reference evapotranspiration under inaccurate data conditions. *Irrigation and drainage systems*, 16, 33-45.

Easterling, D. R., Wallis, T. W., Lawrimore, J. H., & Heim Jr, R. R. (2007). Effects of temperature and precipitation trends on US drought. *Geophysical Research Letters*, 34(20).

Efron, B., & Tibshirani, R. J. (1993). An Introduction to the Bootstrap. Chapman and Hall, 436 pp.

Eyring, V., Bony, S., Meehl, G. A., Senior, C. A., Stevens, B., Stouffer, R. J., & Taylor, K. E. (2016). Overview of the Coupled Model Intercomparison Project Phase 6 (CMIP6) experimental design and organization. *Geoscientific Model Development*, 9(5), 1937-1958.

Fahim, A. M., Ali, S. M., Runping, S., & Zhang, J. (2016). Characteristics of drought variation in winter using drought Indices during the period 1971-2010: A case study of Khyber Pakhtunkhwa (Pakistan). *Mausam*, 67(3), 697-708.

FAO (2022) Statistical Yearbook 2022. *FAO*.

FAO (2024). FAO rapidly responds to severe drought in Viet Nam. https://www.fao.org/vietnam/news/detail-events/ru/c/416018/. (Accessed online on 5 April 2024).

Frees, E. W., & Valdez, E. A. (1998). Understanding relationships using copulas. *North American actuarial journal*, 2(1), 1-25.

Fu, R., Wang, C., Ma, D., Gu, H., Xie, Q., Liu, G., & Yin, G. (2023). Attribution of air temperature and precipitation to the future global drought events. *Environmental Research Communications*, 5(6), 061005.

Gao, Y., Lu, J., & Leung, L. R. (2016). Uncertainties in projecting future changes in atmospheric rivers and their impacts on heavy precipitation over europe. *Journal of Climate*, 29(18), 6711–6726.

Griffin, D., & Anchukaitis, K. J. (2014). How unusual is the 2012–2014 California drought?. *Geophysical Research Letters*, 41(24), 9017-9023.

Ha, N. T. T., Nhuan, M. T., Ngo-Thi, D., & Thao, N. T. P. (2021). Drought disaster in the Central Highlands of Vietnam: Relationship between land-use change and drought impact. In *Proceedings of the 3rd Global Summit of Research Institutes for Disaster Risk Reduction 3* (pp. 241-250). Springer Singapore.

Hargreaves G.H. (1994). Defining and using reference

evapotranspiration. *Journal of Irrigation and Drainage Engineering* 120: 1132–1139.

Hausfather, Z., Marvel, K., Schmidt, G. A., Nielsen-Gammon, J. W., & Zelinka, M. (2022). Climate simulations: Recognize the 'hot model' problem. *Nature*, 605(7908), 26–29.

Hauser, M., Engelbrecht, F., & Fischer, E. M. (2021). Transient global warming levels for CMIP5 and CMIP6 (Version v0.2.0) [Data set]. Zenodo. http://doi.org/10.5281/zenodo.3591807

Im, E. S., Ahn, J. B., & Kim, D. W. (2012). An assessment of future dryness over Korea based on the ECHAM5-RegCM3 model chain under A1B emission scenario. *Asia-Pacific Journal of Atmospheric Sciences*, 48, 325-337.

IPCC (2021). Climate Change 2021: The Physical Science Basis. Contribution of Working Group I to the Sixth Assessment Report of the Intergovernmental Panel on Climate Change[Masson-Delmotte, V., P. Zhai, A. Pirani, S.L. Connors, C. Péan, S. Berger, N. Caud, Y. Chen, L. Goldfarb, M.I. Gomis, M. Huang, K. Leitzell, E. Lonnoy, J.B.R. Matthews, T.K. Maycock, T. Waterfield, O. Yelekçi, R. Yu, and B. Zhou (eds.)]. Cambridge University Press, Cambridge, United Kingdom and New York, NY, USA.

Kelley, C. P., Mohtadi, S., Cane, M. A., Seager, R., & Kushnir, Y. (2015). Climate change in the Fertile Crescent and implications of the recent Syrian drought. *Proceedings of the national Academy of Sciences*, 112(11), 3241-3246.

Kendall, M. G. (1948). Rank correlation methods, Charles Griffin, London, p. 202.

Kotz, M., Lange, S., Wenz, L., & Levermann, A. (2024). Constraining the pattern and magnitude of projected extreme precipitation change in a multimodel ensemble. *Journal of Climate*, 37(1), 97–111.

Kwon, H. H., & Lall, U. (2016). A copula-based nonstationary frequency analysis for the 2012–2015 drought in California. *Water Resources Research*, 52(7), 5662-5675.

Le, P. V. V., Phan□Van, T., Mai, K. V., & Tran, D. Q. (2019). Space–time variability of drought over Vietnam. *International Journal of Climatology*, 39(14), 5437–5451.

Le, M.-H., Kim, H., Moon, H., Zhang, R., Lakshmi, V., & Nguyen, L.-B. (2020). Assessment of drought conditions over Vietnam using standardized precipitation evapotranspiration index, MERRA-2 re-analysis, and dynamic land cover. *Journal of Hydrology: Regional Studies*, 32, 100767.

Le, T., Sun, C., Choy, S., & Kuleshov, Y. (2021). Regional drought risk assessment in the central highlands and the south of vietnam. *Geomatics, Natural Hazards and Risk*, 12(1), 3140–3159.

Li, Z., Shao, Q., Tian, Q., & Zhang, L. (2020). Copula-based drought severity-area-frequency curve and its uncertainty, a case study of Heihe River basin, China. *Hydrology Research*, 51(5), 867-881.

Lloyd-Hughes, B. (2014). The impracticality of a universal drought definition. *Theoretical and applied climatology*, 117, 607-611.

Mann, H. (1945). Non-Parametric Tests against Trend. *Econmetrica*, 13, 245–259.

McKee, T.B., Doesken, N.J. and Kleist, J. (1993). The Relationship of Drought Frequency and Duration to Time Scales. *8th Conference on Applied Climatology, Anaheim*, 17-22 January 1993, 179-184.

Ministry of Planning and Investment (MPI) (2021). National Green Growth Strategy for 2021-2030, vision towards 2050. Retrieved at:https://sustainabledevelopment.gov.mt/wp-content/uploads/2024/10/National-Green-Growth-Strategy-for-2021-2030-Vision-Towards-2050.pdf

Ministry of Agriculture and Rural Development (MARD) (2002). Vietnam National Action Program to Combat Desertification. Retrieved at: https://www.unccd.int/sites/default/files/naps/vietnam-eng2002.pdf

NASA Shuttle Radar Topography Mission (SRTM) (2013). Shuttle Radar Topography Mission (SRTM) Global. Distributed by OpenTopography. https://doi.org/10.5069/G9445JDF. Accessed: 2025-01-09.

Naumann, G., Alfieri, L., Wyser, K., Mentaschi, L., Betts, R. A., Carrao, H., Spinoni, J., Vogt, J., & Feyen, L. (2018). Global changes in drought conditions under different levels of warming. *Geophysical Research Letters*, 45(7), 3285–3296.

Ngo-Duc, T., Nguyen-Duy, T., Desmet, Q., Trinh-Tuan, L., Ramu, L., Cruz, F., Dado, J. M., Chung, J. X., Phan-Van, T., Pham-Thanh, H., Truong-Ba, K., Tangang, F. T., Juneng, L., Santisirisomboon, J., Srisawadwong, R., Permana, D., Linarka, U. A., & Gunawan, D. (2024). Performance ranking of multiple CORDEX-SEA sensitivity experiments: towards an optimum choice of physical schemes for RegCM over Southeast Asia. *Climate Dynamics*, 62(9), 8659-8673.

Nguyen-Duy, T., Ngo-Duc, T., & Desmet, Q. (2023). Performance evaluation and ranking of CMIP6 global climate models over Vietnam. *Journal of Water and Climate Change*, 14(6), 1831-1846.

Nguyen, D. N. & Nguyen, T. H. (2004). Vietnamese climate and climatic resources. (Hanoi Agriculture Press, 2004) (in Vietnamese).

Nguyen, H., & Shaw, R. (2011). Chapter 8 drought risk management in Vietnam. In *Droughts in Asian monsoon region* (pp. 141-161). Emerald Group Publishing Limited.

Persad, G. G., Swain, D. L., Kouba, C., & Ortiz-Partida, J. P. (2020). Inter-model agreement on projected shifts in California hydroclimate characteristics critical to water management. *Climatic Change*, 162(3), 1493–1513.

Phan-Van, T., Nguyen-Ngoc-Bich, P., Ngo-Duc, T., Vu-Minh, T., Le, P. V. V., Trinh-Tuan, L., Nguyen-Thi, T., Pham-Thanh, H., & Tran-Quang, D. (2022). Drought over southeast asia and its association with large-scale drivers. *Journal of Climate*, 35(15), 4959–4978.

Poonia, V., Jha, S., & Goyal, M. K. (2021). Copula based analysis of meteorological, hydrological and agricultural drought characteristics across Indian river basins. *International Journal of Climatology*, 41(9), 4637-4652.

Prudhomme, C., Giuntoli, I., Robinson, E. L., Clark, D. B., Arnell, N. W., Dankers, R., Fekete, B. M., Franssen, W., Gerten, D., Gosling, S. N., Hagemann, S., Hannah, D. M., Kim, H., Masaki, Y., Satoh, Y., Stacke, T., Wada, Y., & Wisser, D. (2014). Hydrological droughts in the 21st century, hotspots and uncertainties from a global multimodel ensemble experiment. *Proceedings of the National Academy of Sciences*, 111(9), 3262–3267.

Riahi, K., van Vuuren, D. P., Kriegler, E., Edmonds, J., O'Neill, B. C., Fujimori, S., Bauer, N., Calvin, K., Dellink, R., Fricko, O., Lutz, W., Popp, A., Cuaresma, J. C., KC, S., Leimbach, M., Jiang, L., Kram, T., Rao, S., Emmerling, J., ... Tavoni, M. (2017). The Shared Socioeconomic Pathways and their energy, land use, and greenhouse gas emissions implications: An overview. *Global environmental change*, 42, 153-168.

Schwarz, G. (1978). Estimating the dimension of a model. *The annals of statistics*, 6(2), 461-464.

Sheffield, J., Wood, E. F., & Roderick, M. L. (2012). Little change in global drought over the past 60 years. *Nature*, 491(7424), 435-438.

Shiau, J. T. (2006). Fitting drought duration and severity with two-dimensional copulas. *Water resources management*, 20, 795-815.

Shiau, J. T., & Modarres, R. (2009). Copula-based drought severity-duration-frequency analysis in Iran. *Meteorological Applications: A journal of forecasting, practical applications, training techniques and modelling*, 16(4), 481-489.

Sklar, K. (1959). Fonctions de repartition à n Dimensions et Leura Marges, *Publ. Inst. Stat. Univ. Paris*, 8, 229–231.

Sun, C., Zhu, L., Liu, Y., Hao, Z., & Zhang, J. (2021). Changes in the drought condition over northern East Asia and the connections with extreme temperature and precipitation indices. *Global and Planetary Change*, 207, 103645.

Tam, B. Y., Cannon, A. J., & Bonsal, B. R. (2023). Standardized precipitation evapotranspiration index (SPEI) for Canada: assessment of probability distributions. *Canadian Water Resources Journal/Revue canadienne des ressources hydriques*, 48(3), 283-299.

Tangang, F., Chung, J. X., Juneng, L., Supari, Salimun, E., Ngai, S. T., Jamaluddin, A. F., Mohd, M. S. F., Cruz, F., Narisma, G., Santisirisomboon, J., Ngo-Duc, T., Van Tan, P., Singhruck, P., Gunawan, D., Aldrian, E., Sopaheluwakan, A., Grigory, N., Remedio, A. R. C., ... Kumar, P. (2020). Projected future changes in rainfall in Southeast Asia based on CORDEX–SEA multi-model simulations. *Climate Dynamics*, 55, 1247-1267.

Thornthwaite, C. W. (1948). An approach toward a rational classification of climate. *Geographical review*, 38(1), 55-94.

Touma, D., Ashfaq, M., Nayak, M. A., Kao, S. C., & Diffenbaugh, N. S. (2015). A multi-model and multi-index evaluation of drought characteristics in the 21st century. *Journal of Hydrology*, 526, 196-207.

Tran-Anh, Q., Ngo-Duc, T., Espagne, E., & Trinh-Tuan, L. (2023). A 10-km CMIP6 downscaled dataset of temperature and precipitation for historical and future Vietnam climate. *Scientific Data*, 10(1), 257.

Tran-Anh, Q., Ngo-Duc, T., Nguyen-Xuan, T. (2024). Changes in Temperature and Rainfall Extremes in Vietnam under Progressive Global Warming Levels from 1.5°C to 4°C. *Submitted to AFD research papers*.

Trenberth, K. E., Dai, A., Van Der Schrier, G., Jones, P. D., Barichivich, J., Briffa, K. R., & Sheffield, J. (2014). Global warming and changes in drought. *Nature Climate Change*, 4(1), 17–22.

Ukkola, A. M., De Kauwe, M. G., Roderick, M. L., Abramowitz, G., & Pitman, A. J. (2020). Robust future changes in meteorological drought in CMIP6 projections despite uncertainty in precipitation. *Geophysical Research Letters*, 47(11), e2020GL087820.

United Nations Food Systems Summit (UNFSS) (2021). Second National Dialogue toward the UN 2021 Food Systems Summit. Retrieved at: https://summitdialogues.org/dialogue/35195/

United Nations Environment Programme (2024). Executive summary. In Emissions Gap Report 2024: No more hot air ... please! With a massive gap between rhetoric and reality, countries draft new climate commitments. Nairobi.

Vicente-Serrano, S. M., Begueria, S., & Lopez-Moreno, J. I. (2010). A multiscalar drought index sensitive to global warming: the standardized precipitation evapotranspiration index. *Journal of climate*, 23(7), 1696-1718.

Vicente-Serrano, S. M., Lopez-Moreno, J.-I., Beguería, S., Lorenzo-Lacruz, J., Sanchez-Lorenzo, A., García-Ruiz, J. M., Azorin-Molina, C., Morán-Tejeda, E., Revuelto, J., Trigo, R., Coelho, F., & Espejo, F. (2014). Evidence of increasing drought severity caused by temperature rise in southern Europe. *Environmental Research Letters*, 9(4), 044001.

Vietnam Organizational Structure of the National Steering Committee (OSNSC) (2021). A year with historical drought (ONSC, 3 January 2021). https://phongchongthientai.mard.gov.vn/en/Pages/a-year-with-historical-drought.aspx (Accessed online on 5 April 2024).

Vu-Thanh, H., Ngo-Duc, T., & Phan-Van, T. (2014). Evolution of meteorological drought characteristics in Vietnam during the 1961–2007 period. *Theoretical and Applied Climatology*, 118, 367-375.

Wang, Q., Wu, J., Lei, T., He, B., Wu, Z., Liu, M., Mo, X., Geng, G., Li, X., Zhou, H., & Liu, D. (2014). Temporal-spatial characteristics of severe drought events and their impact on agriculture on a global scale. *Quaternary International*, 349, 10-21.

Wilhite, D. A., & Glantz, M. H. (1985). Understanding: the drought phenomenon: the role of definitions. *Water international*, 10(3), 111-120.

Wilhite, D. A. (2000). Drought as a Natural Hazard: Concepts and Definitions. In D. Wilhite (Ed.), Drought: A Global Assessment (Vol. 1, pp. 3-18). London: Routledge.

World Bank Group (2022) Vietnam Country Climate and Development Report. World Bank Group Country Climate and Development Report. Retrieved at:https://documents1.worldbank.org/curated/en/099355507062229876/pdf/P177241030 36ee07909701028a237b6d18b.pdf

World Trade Organization (WTO) (2023) World Trade Report 2024: Re-globalization for a secure, inclusive and sustainable future, Geneva:WTO. Retrieved at: https://www.wto.org/english/res_e/booksp_e/wtr23_e/wtr23_e.pdf

Yue, Y., Liu, H., Mu, X., Qin, M., Wang, T., Wang, Q., & Yan, Y. (2021). Spatial and temporal characteristics of drought and its correlation with climate indices in Northeast China. *PLoS One*, 16(11), e0259774.

Zappa, G., Ceppi, P., and Shepherd, T (2021). Time-evolving sea-surface warming patterns modulate the climate change response of precipitation in Mediterranean-like regions. *EGU General Assembly 2021*, online, 19–30 Apr 2021, EGU21-13493.

Zhao, T., & Dai, A. (2022). CMIP6 model-projected hydroclimatic and drought changes and their causes in the twenty-first century. *Journal of Climate*, 35(3), 897-921.

List of acronyms and abbreviations

AFD	Agence Française de Développement
AR6	Sixth Assessment Report
BCSD	Bias Correction and Spatial Disaggregation
CMIP5	Coupled Model Intercomparison Project Phase 5
CMIP6	Coupled Model Intercomparison Project Phase 6
CWB	Climatic Water Balance
ECS	Equilibrium Climate Sensitivity
EDI	Effective Drought Index
FAO	Food and Agriculture Organization of the United Nations
FDD	Frequency Density Distribution
GCM	Global Climate Models
GWL	Global Warming Levels
IPCC	Intergovernmental Panel on Climate Change
NAP	National Action Programme
PET	Potential EvapoTranspiration
SPEI	Standardized Precipitation-Evapotranspiration Index
SPI	Standardized Precipitation Index
SSP	Shared Socioeconomic Pathway
UNESCO	United Nations Educational, Scientific and Cultural Organization
UNFSS	United Nations Food System Summit
VnGC	Vietnam Gridded Climate Dataset

Appendix

A.1. Statistics on the number of available models for each Global Warming Levels

Table S1. Statistics on the number of available models for each Global Warming Levels

GWLs	Total available models	Available models of SSP1-2.6 / SSP2-4.5 / SSP5-8.5
1.5	33	9 / 12 / 12
2.0	53	12 / 21 / 20
3.0	31	0 / 10 / 21
4.0	15	0 / 1 / 14

A.2. Temporal evolution of area-averaged SPEI-12

Figure S1. Temporal evolution of area-averaged SPEI-12 for the seven sub-climatic regions under SSP5-8.5, projected by the downscaled product of HadGEM3-GC31-LL. The red-dashed lines indicate the -0.5 threshold, which is used to detect drought events.

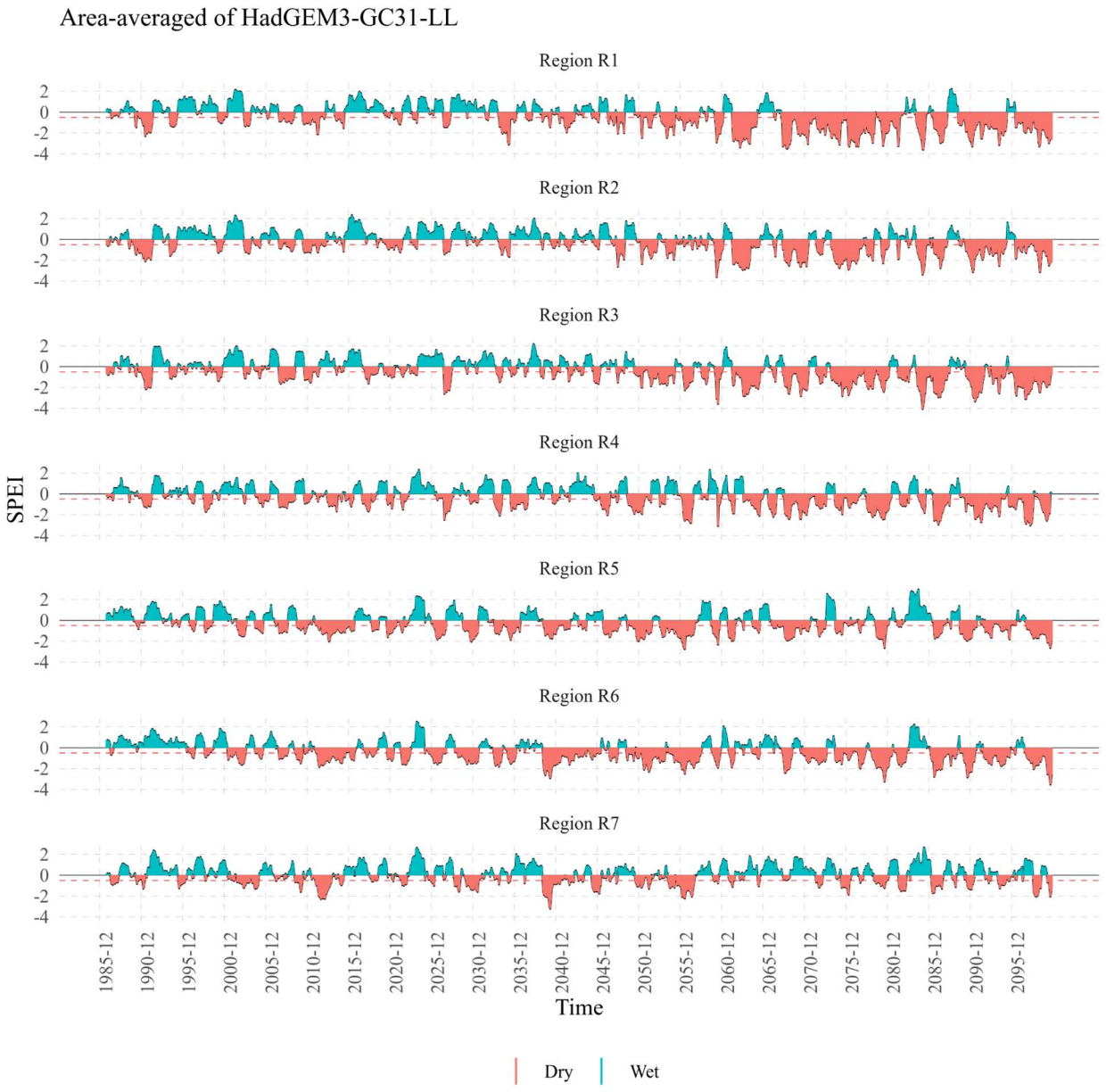

Figure S2. Similar to Figure S1, but for EC-Earth3-Veg.

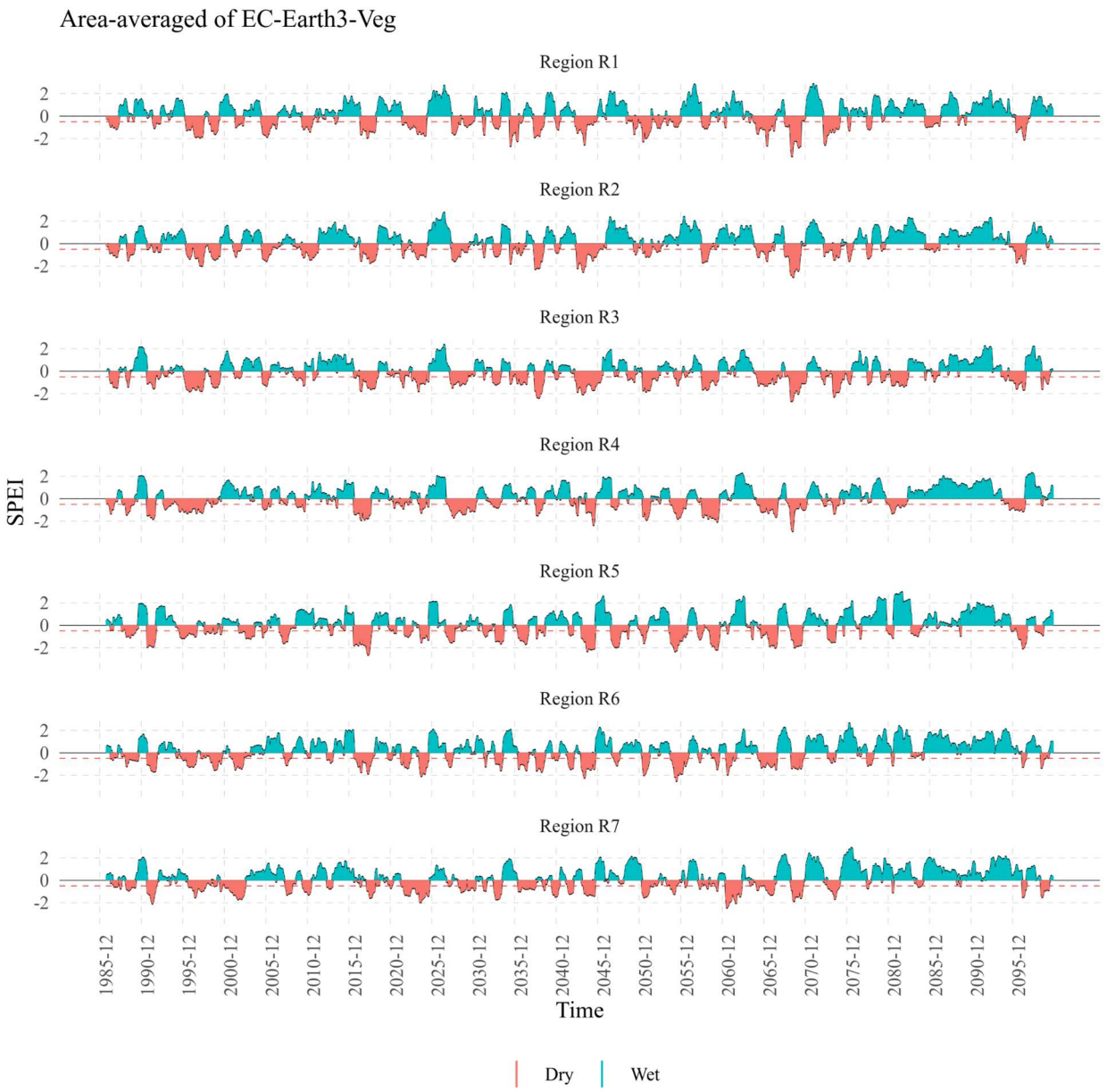

Figure S3. Similar to Figure 12, but the difference values have been tested for statistical significance using the bootstrap technique. Hatched areas indicate regions where changes are statistically insignificant (i.e., the p-value reported from the bootstrap test is greater than 0.05).

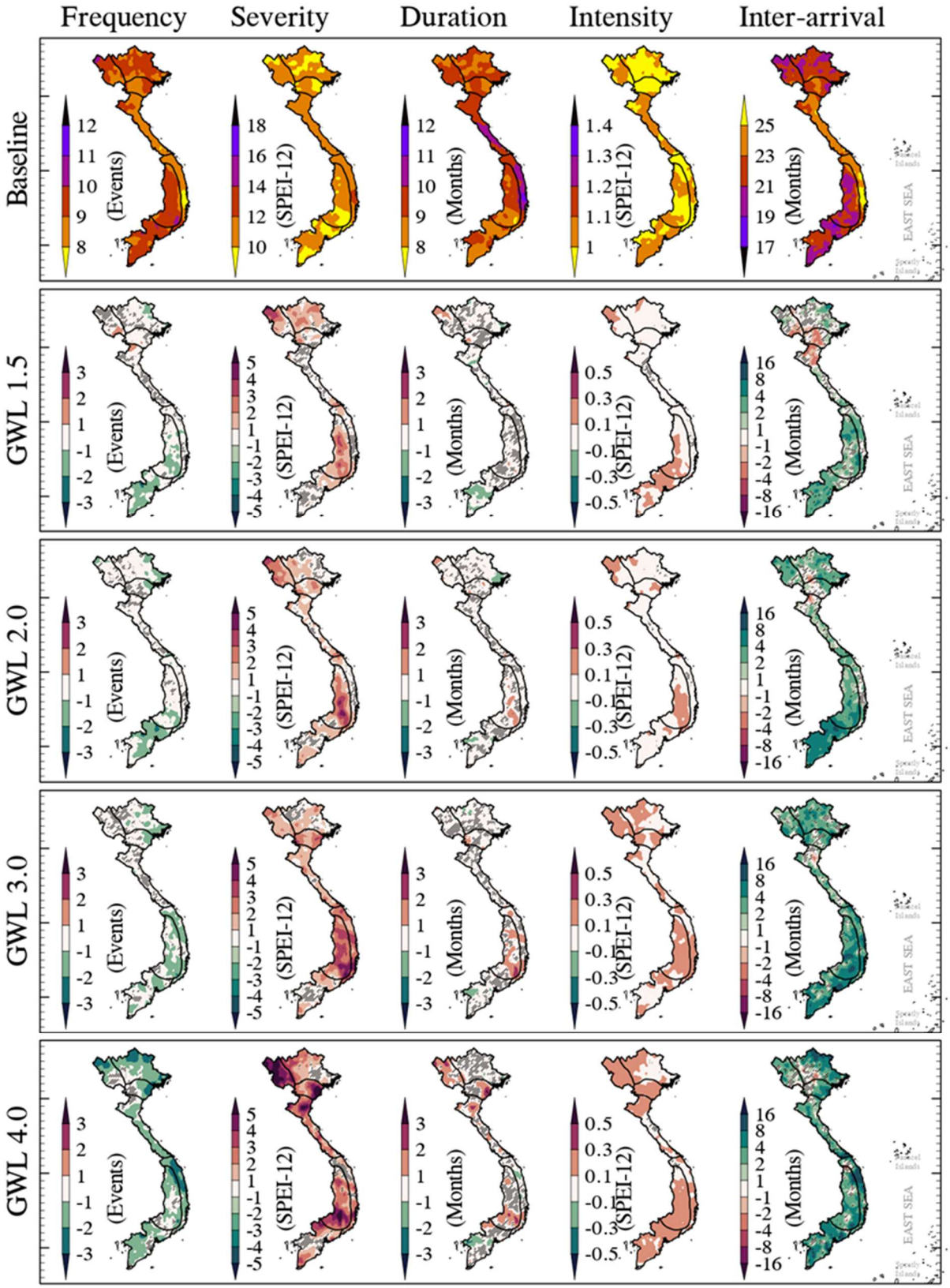

Agence française
de développement
5, rue Roland Barthes
75012 Paris I France
www.afd.fr

What is AFD?
Éditions Agence française de développement publishes analysis and research on sustainable development issues. Conducted with numerous partners in the Global North and South, these publications contribute to a better understanding of the challenges faced by our planet and to the implementation of concerted actions within the framework of the Sustainable Development Goals.
With a catalogue of more than 1,000 titles and an average of 80 new publications published every year, Éditions Agence française de développement promotes the dissemination of knowledge and expertise, both in AFD's own publications and through key partnerships. Discover all our publications in open access at editions.afd.fr.
Towards a world in common.

Publication Director Rémy Rioux
Editor-in-Chief Thomas Melonio

Legal deposit 2nd[t] quarter 2025
ISSN 2492 - 2846

Rights and permissions
Creative Commons license
Attribution - No commercialization - No modification
https://creativecommons.org/licenses/by-nc-nd/4.0/

Graphic design MeMo, Juliegilles, D. Cazeils
Layout PUB
Printed by the AFD reprography service

To browse our publications:
https://www.afd.fr/en/ressources-accueil